Magnetic Resonance Spectroscopic Imaging Technique to Measure Dynamic Metabolism

January 2015

Yoshitaka Bito

Graduate School of Engineering

CHIBA UNIVERSITY

（千葉大学審査学位論文）

Magnetic Resonance Spectroscopic Imaging Technique to Measure Dynamic Metabolism

January 2015

Yoshitaka Bito

Graduate School of Engineering

CHIBA UNIVERSITY

CONTENTS

ABSTRACT

Magnetic resonance spectroscopic imaging (MRSI) is a very useful technique for both clinical diagnosis and basic medical science to investigate metabolism *in vivo*. Recently, research on dynamic metabolism, which is to investigate metabolism while taking time into account, has been expanding to measure change of metabolite distribution through time and to measure chemical exchange rate or transport of metabolites.

This thesis focused on development of fast and accurate MRSI techniques for two researches on dynamic metabolism: (1) measuring rapid changes in lactate distribution to observe anaerobic metabolism and (2) measuring molecular diffusion of metabolites to observe microscopic transport of metabolites. Fast echo-planar spectroscopic imaging (EPSI) technique was used as basic technique for both aims. According to (1), echo-shift technique was developed with EPSI to discriminate lactate from contaminated lipid signal. According to (2), diffusion-weighted EPSI and diffusion-weighted line-scan EPSI were developed to reduce measurement time as well as motion artifacts for improved accuracy in imaging metabolite diffusion.

Improved measurement speed (several to several ten times) and increased accuracy were demonstrated by applying these techniques to phantoms and rats *in vivo*. These techniques were expected to be a powerful tool in investigating microscopic dynamic metabolism and in early diagnosing subtle metabolic changes of diseases.

ACKNOWLEDGEMENTS

I would firstly like to express my deeply thank to my supervisor Professor Etsuji Yamamoto of Chiba University. This research would never have taken shape without not only his academic profession, but also his thoughtful direction at my entering research on magnetic resonance imaging and his open minded act for collaborative research with academic societies when he worked for Hitachi, Ltd. I would also like to express my gratitude to Professor Hideaki Haneishi, Professor Tatsuo Igarashi, Professor Tadashi Yamaguchi and Associate Professor Mikio Suga of Chiba University for their expert guidance and advice.

I would like to thank all researchers at Hitachi, Ltd. including Satoshi Hirata, Takayuki Nabeshima, Yukari Yamamoto, Dr. Koji Hirata, Yosuke Otake, Toru Shirai, Dr. Yoshihisa Soutome, and Dr. Hisaaki Ochi for their various supports about the research. Especially, their effort in developing cutting-edge MRI systems, 4.7-T and 7–T MRI for small animal study, was essential for the research. I would like to thank all researchers at collaborative universities including Dr. Toshihiko Ebisu, Dr. Masahiro Umeda, Dr. Toshihiro Higuchi, Dr. Chuzo Tanaka at Meiji University of Integrative Medicine, and Dr. Tetsuro Takegami and Dr. Shoji Naruse at Kyoto Prefectural University of Medicine for their valuable discussion from medical perspective and for their high motivation to proceed this research.

I would lastly like to thank my wife Kazumi and my son Ryo for encouraging me to perform this research. I never would have finished this research without their kind supports.

CHAPTER 1 INTRODUCTION

1.1 BACKGROUND

1.1.1 MAGNETIC RESONANCE SPECTROSCOPY AND SPECTROSCOPIC IMAGING

Magnetic resonance imaging (MRI) is very useful for clinical diagnosis and medical research because it can provide rich biological information about soft tissues. The obtainable biological information includes relaxation time, chemical shift, fluid flow, molecular diffusion, magnetic susceptibility, temperature, and so on. The major advantage of MRI is that such various biological information can be obtained by just modifying measurement technique in software: pulse sequence and data processing.

Magnetic resonance spectroscopy (MRS) is a measurement technique to obtain concentration of every metabolites separated by difference of magnetic resonant frequency called chemical shift [1, 2] (Fig. 1.1). The chemical shift is caused by additional magnetic field which is generated by surrounding electrons of molecules, and thus the chemical shift can be used to distinguish molecules. Time-series signal is measured and applied one-dimensional Fourier transform to obtain spectra of metabolites. Typical obtainable metabolites *in vivo* are N-acetylaspartate (NAA), creatine (Cr), choline containing compounds (Cho), lactate (Lac), myo-inositole (mIns). The concentration of these metabolites is expected to provide important information about biological tissues. For example, brain cancer decreases concentration of NAA and increases concentrations of Cho and Lac according to malignancy. Magnetic resonance spectroscopic imaging (MRSI) is a hybrid technique of MRS and basic imaging

technique of MRI to map metabolite distribution (Fig. 1.2). Typically, three-dimensional hybrid data in (time, k_x, k_y)-space, i.e. time for MRS and (k_x, k_y) for basic imaging technique, is measured and applied three-dimensional Fourier transform to obtain spectroscopic image. The spectroscopic image has both spectral and spatial information including distribution maps of metabolites and spectra at spatial voxels. Although MRS can provide metabolite concentration at small region of interest, MRSI can further provide distribution of metabolite. The spatial variation of metabolite concentration is expected to provide important information about biological tissue such as infiltration of cancer.

Although MRS and MRSI provide important metabolic information, these techniques were not used for clinical diagnosis so often. This was because MRS and MRSI had disadvantages in signal-to-noise ratio (SNR), measurement time, and spatial resolution. Furthermore, correction of static magnetic field adapted to biological tissues *in vivo* was not easy to obtain sufficient spectral resolution. These disadvantages limited their clinical use because it was difficult to obtain sufficient accuracy in some clinical settings. For example, setting long measurement time increased SNR but contrary increased artifacts induced by patient motion.

Recently improved hardware and software have overcome these disadvantages of MRS and MRSI to some extent. Increased static magnetic field, 3 T in clinical use and higher than 7 T in research use, has increased SNR. Dedicated radio frequency (RF) coils tuned well to the target biological tissue has also increased SNR. Fast measurement and calculation software for correction of static magnetic field inhomogeneity has increased spectral resolution as well as SNR. Increased SNR can be

used to reduce measurement time and spatial resolution. And thus, MRS and MRSI have been used for clinical diagnosis of some cancers: brain, breast and prostate, and congenital metabolic diseases.

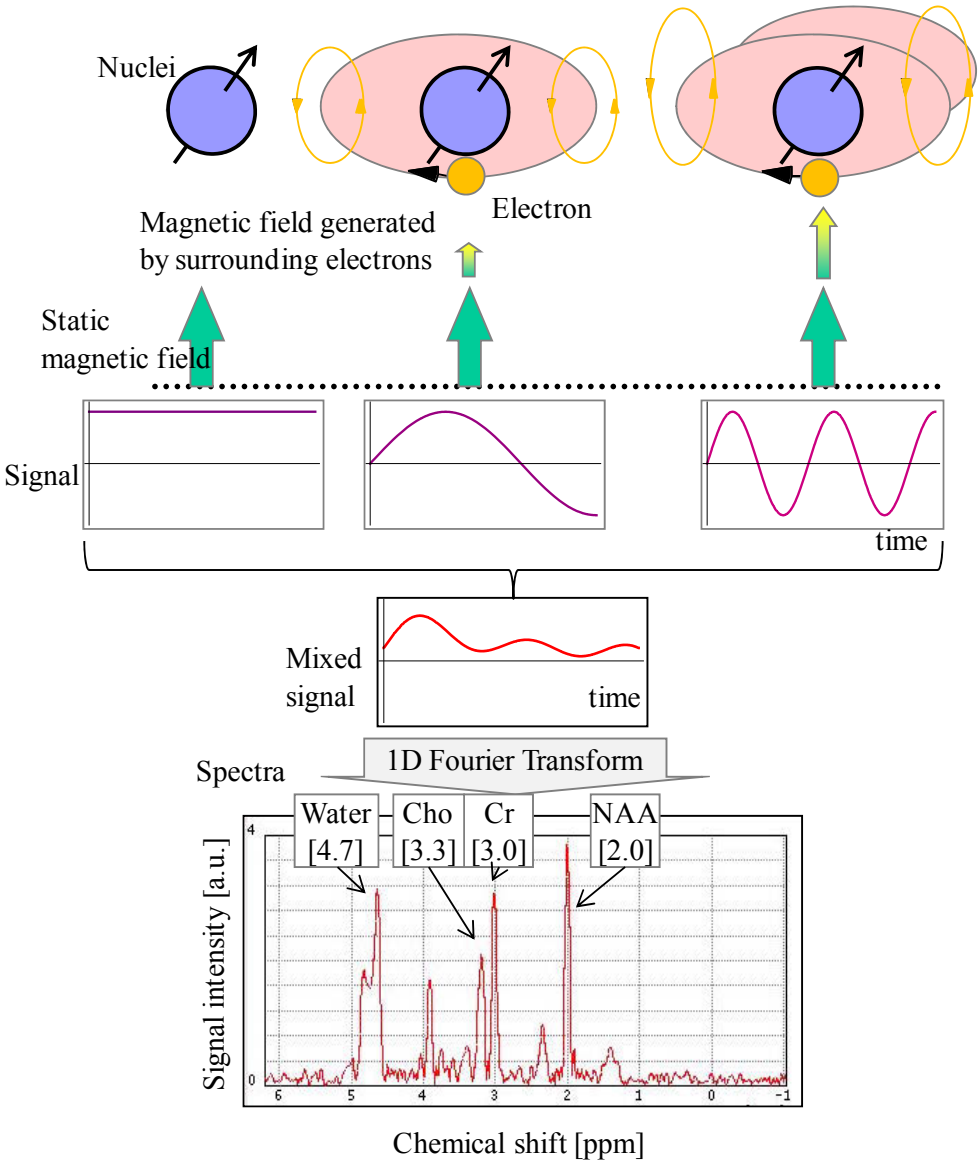

Figure 1.1. Schematic diagram of measurement mechanism of magnetic resonance spectroscopy (MRS). Magnetic resonant frequency of nuclei varies in molecule due to surrounding electrons. Measured mixed signal of metabolites is one-dimensional Fourier transformed to spectra of which difference in frequency is called chemical shift.

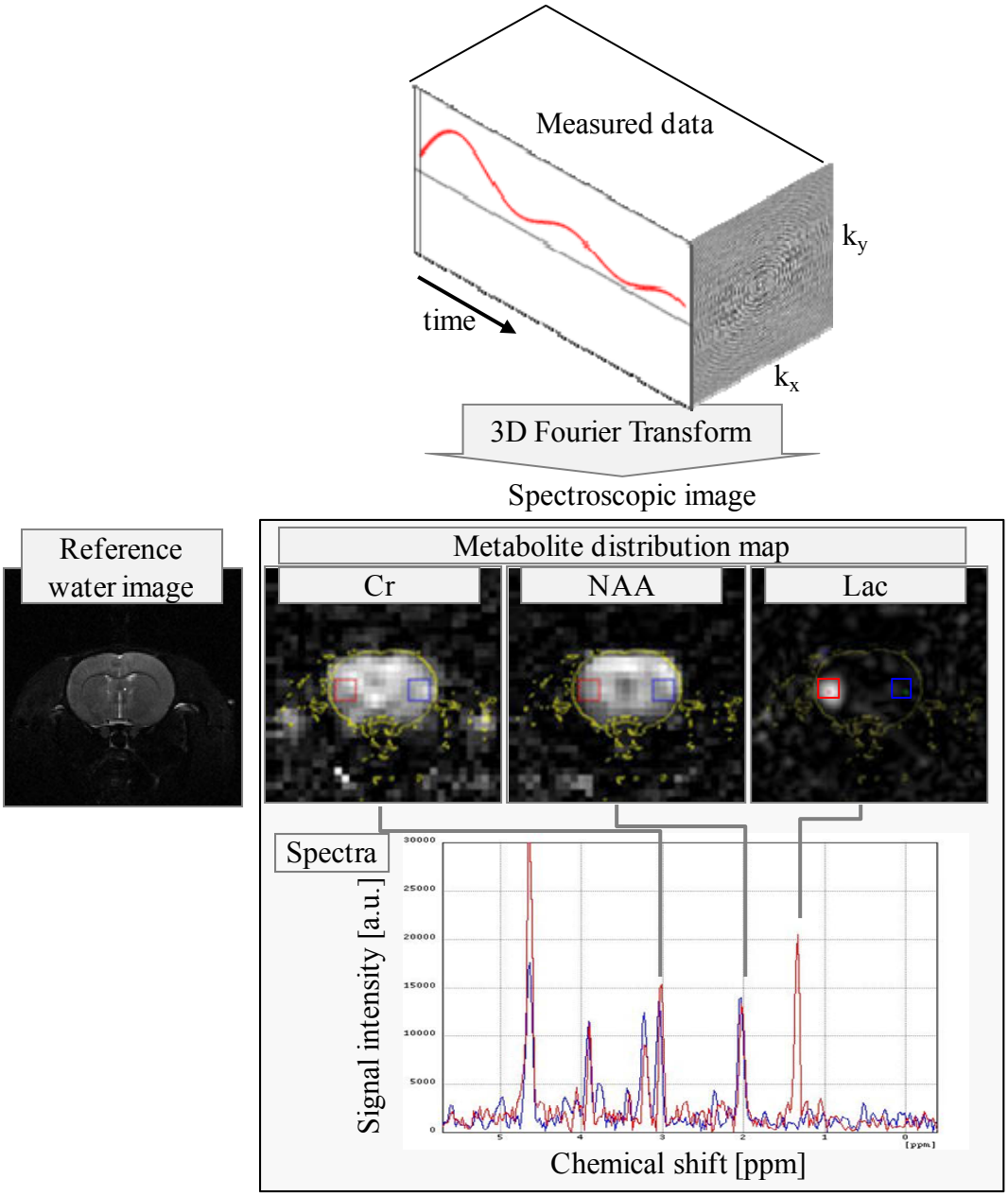

Figure 1.2. Schematic diagram of measurement mechanism of magnetic resonance spectroscopic imaging (MRSI). Data in (time, k_x, k_y)-space, hybrid of time for MRS and (k_x, k_y) for conventional imaging, is three-dimensional Fourier transformed to a spectroscopic image. The spectroscopic image shows distribution maps of metabolites such as N-acetylaspartate (NAA), Creatine (Cr), and lactate (Lac), and spectra of spatial voxels indicated as red and blue rectangles on the distribution maps.

1.1.2 RESEARCH ON DYNAMIC METABOLISM

The improved hardware and software enable not only clinical use of MRS and MRSI but also expanding research on dynamic metabolism which takes time into account with MRS and MRSI. Most clinical MRS and MRSI are taken as measurement of static metabolism because obtained metabolism in cancer or congenital metabolic diseases are not thought to be varied through time so rapidly. In contrast to that, dynamic metabolism takes time into account, which means observing change of metabolite concentration through time, and observing chemical exchange rate of metabolites i.e. exchanging amount divided by time. The research on dynamic metabolism can be categorized from the view of target metabolic phenomena and target molecule (Fig 1.3, Table 1.1). There are two categories from the view of metabolic phenomena: (1) rapid change of metabolite concentration, and (2) chemical exchange rate and transport of metabolite even though the concentration of metabolite seems to be static. According to (1), MRS and MRSI enable detecting concentration of each metabolite. According to (2), MRS and MRSI with basic imaging technique of MRI, such as flow measurement technique and molecular diffusion measurement technique, enable detecting movement of each metabolite. There are also two categories from the view of target molecule to be measured: (a) endogenous molecule such as NAA, Cho, Cr, and Lac, and (b) exogenous molecule such as ^{13}C-labeled glucose, ^{19}F-labeled drugs and molecules labeled with paramagnetic particle. Advantages using exogenous molecule are that chemical exchange rate can be observed even though the concentration of natural abundant molecule seems to be stable, SNR can be dramatically increased by hyper-polarization, and signal from the exogenous molecule can be easily

identified because of no signal from background. However, dosage of those exogenous molecules may restrict their usage in some clinical settings.

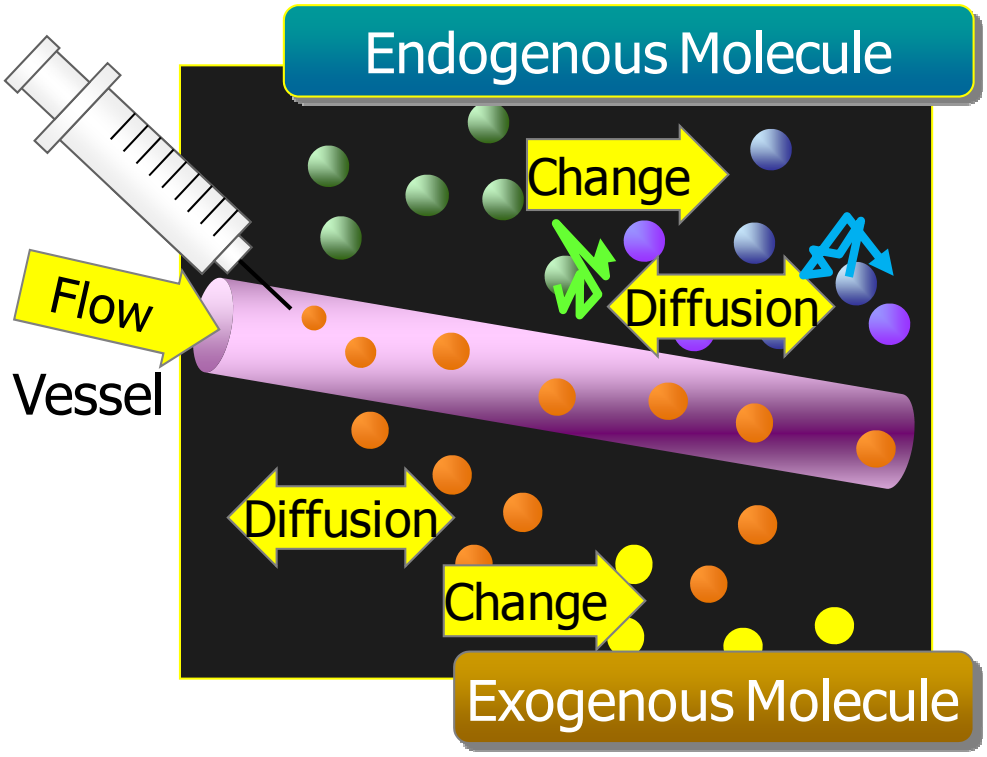

Figure 1.3. Schematic diagram of physiological targets of dynamic metabolism. The targets are chemical exchange, flow and diffusion of endogenous and exogenous molecules.

Table 1.1. Examples of research on dynamic metabolism categorized from the view of target metabolic phenomena and target molecule.

Examples of research		Target metabolic phenomena	
		(1) Concentration change of metabolite	(2) Chemical exchange rate and transport of metabolite
Target molecule	(a) Endogenous molecule Ex) NAA, Cho, Cr, Lac	・Anaerobic metabolism observed by measuring distribution change of Lac after ischemia [3]. ・Brain activity observed by using Lac [4].	・Microscopic transport observed by measuring molecular diffusion of metabolites [5]. ・Chemical exchanging rate observed by using saturation transfer effect of specific metabolites [6]. ・Macroscopic transport observed by measuring flow of metabolites [7].
	(b) Exogenous molecule Ex) ^{13}C-labeld glucose, ^{19}F-labeld drugs	・Drug monitoring by measuring distribution and chemical change of 5-Fluorouracil (^{19}F-labeled anti-cancer drug) for improved cancer therapy [8,9].	・Glycolisys and aerobic metabolism rate observed by using ^{13}C-labeled glucose [10] and hyperpolarized ^{13}C-labeled pyruvate [11]. ・Aerobic metabolism and transport observed by using $^{17}O_2$ inhalation [12]. ・Lung ventilation function observed by measuring hyperpolarized gases [13].

In this thesis, development of MRSI technique for the research on both (1) rapid change of metabolite concentration and (2) chemical exchange rate and transport of metabolite using (a) endogenous molecule were presented.

According to (1) rapid change of metabolite concentration, target study was to investigate dynamic anaerobic metabolism by measuring change of lactate distribution after onset of stroke. Current challenge in stroke diagnosis is to identify ischemic penumbra, which is expected to be partially damaged but salvageable by appropriate care, around ischemic core which is not expected to be reversible. Although diffusion-weighted imaging (DWI) can provide early sign of ischemia; however, region identified by DWI is thought to be the ischemic core. Perfusion-weighted imaging (PWI) can provide information about reduced blood flow; however, region identified by PWI is thought to be larger than the ischemic penumbra because consumption of oxygen is not taken into account in PWI [14]. Lactate elevation is expected to be a biomarker of anaerobic metabolism which occurs in both ischemic core and penumbra, and is expected to be used to identify penumbra by subtracting ischemic core identified by DWI. Thus, fast and accurate MRSI technique is needed to map lactate distribution rapidly both for research to accumulate knowledge about stroke and for clinical diagnosis of acute stroke.

According to (2), target study was to investigate intracellular transport of metabolites by measuring molecular diffusion of metabolites. The intracellular transport is an important biomarker because cytoplasmic streaming is dropped and structure of neuron is changed by energy deficit in stroke. The intracellular transport is also reported to be reduced in Alzheimer's diseases because cytoskeleton is broken and obstructive

proteins are increased [15, 16]. DWI can provide information about diffusion property of water; however, the information is not specific to intracellular property because water also exists in extracellular space. The information about diffusion property of water does not directly reflect diffusion property of metabolites because hindrance is different with molecules. Thus, fast and accurate diffusion-weighted spectroscopic imaging (DWSI) technique is needed to measure diffusion property of metabolites.

Fundamental technical challenge for both (1) and (2) was to develop fast MRSI technique. For this purpose, echo-planar spectroscopic imaging (EPSI) technique was used as basic technique for both (1) and (2) [17, 18]. Major technical challenge according to (1) was to discriminate lactate signal from overlapped lipid signal in the same chemical shift. Echo-shift technique in combination with EPSI was presented to discriminate lactate fast [19]. Major technical challenge according to (2) was to reduce measurement time because various diffusion-weighting was needed to be added on conventional MRSI technique. Diffusion-weighted EPSI (DW-EPSI) was presented for this purpose [20]. Further technical challenge was to suppress motion artifacts caused by respiration and/or pulsation. Line-scan technique with DW-EPSI (DW-LSEPSI) compensating the motion was presented for this purpose [21].

1.2 AIMS OF THIS THESIS

The overall aim of this thesis was to develop MRSI technique for measuring dynamic metabolites using endogenous molecules. There were two specific aims in technical development:

(1) fast and accurate MRSI technique to measure rapid changes of lactate distribution without lipid contamination for observing anaerobic metabolism, and

(2) fast and accurate diffusion-weighted MRSI (DWSI) technique to measure molecular diffusion without motion artifacts caused by respiration and/or pulsation for observing microscopic transport of metabolites.

1.3 OVERVIEW OF THIS THESIS

This thesis divided into two parts according to the two aims; chapter 2 describes technical development to measure rapid changes of lactate distribution, and chapter 3 and 4 describe technical development to measure molecular diffusion of metabolites. Detailed description about each chapter is as follows:

Chapter 2: Fast Spectroscopic Imaging Technique to Measure Lactate Distribution – presents technique to measure rapid changes of lactate distribution accurately. Lactate concentration is one of the important biomarkers for anaerobic metabolism in case of stroke or cancer. Especially in acute stroke, lactate concentration is needed to be measured rapidly because it changes rapidly after onset of ischemia. To acquire lactate distribution fast and accurately, presented technique uses two techniques: (1)

echo-planar spectroscopic imaging (EPSI) technique, which efficiently scans two-dimensional spatio-spectral space by zigzag trajectory, and (2) echo-shift technique, which discriminate lactate signal from overlapped lipid signal by using *J*-coupling in lactate. The presented technique demonstrated fast acquisition of lactate discriminated image from lipid by using rat stroke models *in vivo*.

Chapter 3: Fast Diffusion-weighted Spectroscopic Imaging Technique to Measure Molecular Diffusion – presents technique to acquire molecular diffusion maps in short measurement time. One of the major issues in DWSI is long measurement time because it needs measurement loop for various *b*-values in addition to measurement loops for normal spatio-spectral information. To shorten the measurement time, presented technique uses EPSI technique. The presented technique demonstrates fast acquisition of multi-molecular diffusion maps by using phantom.

Chapter 4: Diffusion-weighted Spectroscopic Imaging Technique to Reduce Motion Artifacts in Metabolites Diffusion Imaging – presents technique to reduce motion artifacts for DWSI. The motion artifacts are signal loss in averaging and ghosting in phase-encoding caused by phase errors induced by respiration and/or pulsation. The presented technique uses line-scan technique in combination with the EPSI technique. The hybrid of the line-scan technique and the EPSI technique enables phase correction at each shot and each point, and thus it leads to reduce motion artifacts. The presented technique demonstrated reduced motion artifacts and reduced measurement time by using normal rat brain *in vivo*.

Chapter 5: Conclusions – presents the overall conclusions of the above research on technical development for dynamic metabolism. It also includes discussion about

potential future direction about technical development and their application in dynamic metabolism.

CHAPTER 2 FAST SPECTROSCOPIC IMAGING TECHNIQUE TO MEASURE LACTATE DISTRIBUTION

2.1 INTRODUCTION

Imaging of lactate distributions can provide useful information about anaerobic metabolism in tissues, enabling an estimate of oxygen shortfall at ischemic region in stroke or at hypoxic region in cancer. Although ^{13}C-labeled lactate can be used, lactate imaging usually uses the ^{1}H chemical shift to separate the lactate signal from other metabolites because natural abundant ^{13}C-labeled lactate is very low and dosage of ^{13}C-labeled exogenous molecule is difficult in most clinical cases. ^{1}H chemical shift can overcome these problems; however, contamination from overlapping lipid signals sometimes makes it difficult to accurately evaluate the lactate concentration. Additional discrimination of the lactate signal from the lipid signal is therefore necessary for obtaining accurate lactate images. Several lactate-discriminating techniques have been reported that use the difference between the relaxation times of lactate and lipid [22, 23] or homonuclear coupling in lactate protons [24-38], and their application to spectroscopic imaging has also been reported [23-29]. The lactate-discriminating techniques using homonuclear coupling can be classified into four categories: selective irradiation [24], spectral editing [23-27], multiple quantum coherence [28, 29], and polarization transfer [30]. These techniques demonstrate the efficiency of lactate discrimination, but there remain some disadvantages with regard to measurement time and to obtaining the spectra of other metabolites. At least two measurements are generally required for selective irradiation, spectral editing or polarization transfer [24-26, 30], and

images of other metabolites cannot be acquired simultaneously when multiple quantum coherence are used [28, 29]. Although the spectral editing technique using multiple spin-echo allows the images of the other metabolites to be simultaneously acquired in a single measurement, sufficient discrimination is sometimes not provided by the T_2 variation of the lipid signal [27].

In this chapter, a fast lactate-discriminating technique for ^{1}H spectroscopic imaging is presented for observing dynamic anaerobic metabolism [19]. This technique enables lactate-discrimination in a single measurement and makes possible the simultaneous acquisition of the spectra of other metabolites. It is based on homonuclear coupling between lactate protons and on the broad bandwidth of lipid spectrum. By using *TE* values determined by n/J (n: a natural number, J: J-coupling constant), the lipid signal can be decreased at the time when the lactate signal is strongest, which means shifting lactate echo peak from lipid echo peak. The echo-shift technique includes data processing to calculate the intensity of lactate signal from the reconstructed spectra. We have developed lactate-discriminating echo-planar spectroscopic imaging (EPSI) technique by combining the echo-shift technique with conventional EPSI technique [17, 18, 39, 40]. The conventional EPSI technique has an advantage on measurement time compared to the 3D-CSI (three-dimensional chemical shift imaging) technique which uses two-dimensional phase-encodings. The conventional EPSI technique reduces measurement time by simultaneously acquiring spectral information and one-dimensional spatial information by using oscillating readout gradient. Acquisition of discriminated lactate images is demonstrated by applying the lactate-discriminating EPSI technique to focal cerebral ischemia in rats.

2.2 MATERIALS AND METHODS

2.2.1 ECHO-PLANAR SPECTROSCOPIC IMAGING TECHNIQUE

Figure 2.1 shows schematic diagrams of the simplest sequence of conventional three-dimensional chemical shift imaging (3D-CSI) using two-dimensional phase encodings, and conventional EPSI technique [17, 18] that is used as a basic technique for this development. It uses a rapidly oscillating gradient in the x-direction simultaneously with data acquisition, and a phase-encode gradient in the y-direction changing its amplitude in steps. The oscillating gradient encodes spatial information in the x-direction and the passage of time encodes spectral information. This technique has an advantage of easy adjustment of parameters, such as echo time or static magnetic field shimming, in prescanning (zero phase-encoding) because chemical shift can be acquired in each scan. In contrast with the 3D-CSI, acquisition time is shorter because the two-dimensional (time, k_x)-plane is scanned all at once.

The data is reconstructed by three-dimensional Fourier transform. Some correction is necessary during reconstruction, as the data points are not on a lattice [41]. For instance, if the shape of the oscillating gradient is designed to be sinusoidal, a sine-correction technique is required because the trajectory of the data points is a sinusoidal function.

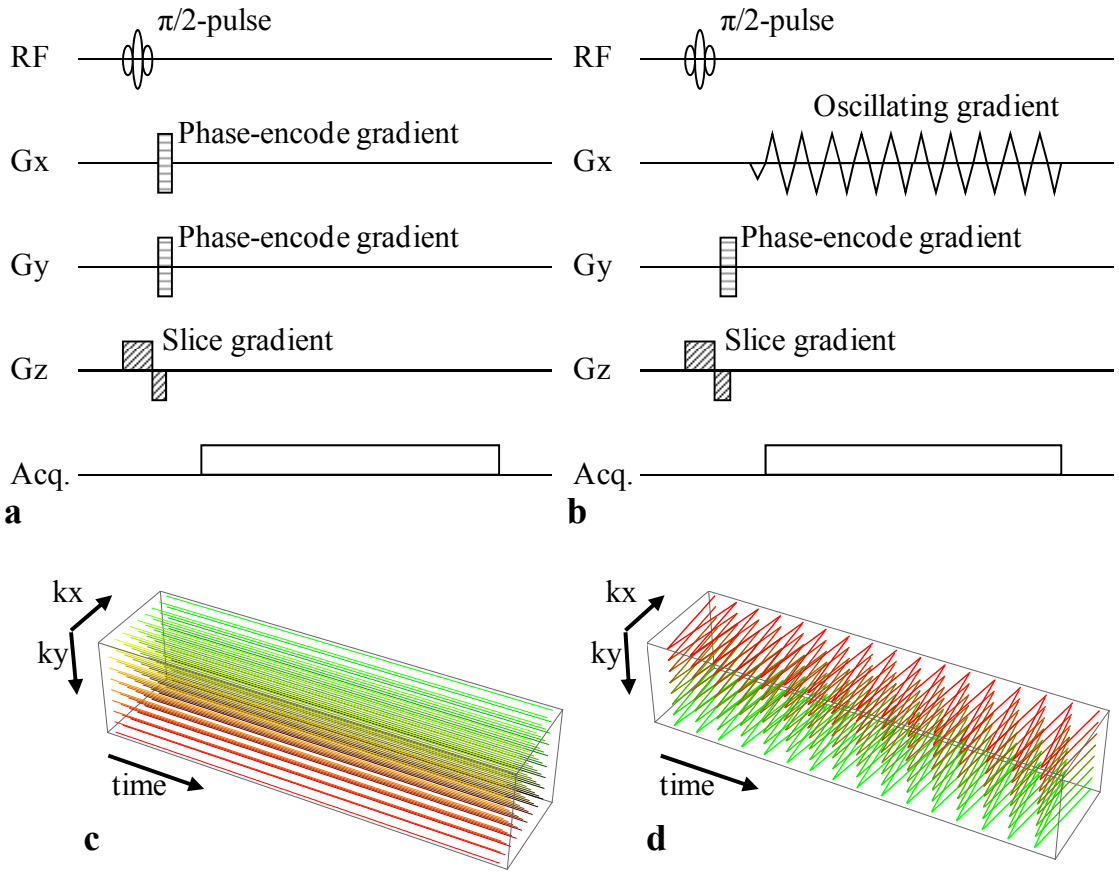

Figure 2.1. Schematic sequence diagrams (**a**, **b**) and trajectories (**c**, **d**) in (time, k_x, k_y)-space of conventional 3D-CSI (three-dimensional chemical shift imaging) technique which uses two-dimensional phase-encodings, and conventional echo-planar spectroscopic imaging technique (EPSI), respectively. EPSI uses rapidly oscillating gradient which encodes both spatial information and one-dimensional spatial information with zigzag trajectory in (time, k_x)-space. It reduces a loop for one dimensional phase encoding.

2.2.2 *LACTATE-DISCRIMINATING ECHO-SHIFT TECHNIQUE*

Figure 2.2 shows the schematic diagram of lactate molecule. The methyl protons (1.3 ppm) show doublet spectrum and the methine proton (4.2 ppm) shows quartet spectrum by the *J*-coupling between the methyl and methine protons. The methyl protons are used to identify lactate because methine proton is difficult to be measured accurately under overlapping large water signal. However, accurate measurement of the methyl protons is also hampered by overlapping lipid signal.

Figure 2.3 illustrates the proposed lactate-discriminating echo-shift technique schematically. The echo-shift technique uses spin-echo technique, i.e. combination of π/2-pulse and π-pulse to generate spin echo. The measurement parameters satisfy the following two conditions: (condition 1) the bandwidth of the two RF pulses is large enough that both the methyl protons (1.3 ppm) and the methine proton (4.2 ppm) of lactate are excited, and (condition 2) *TE* and *n*/*J* are sufficiently separated. Because the π-pulse inverts both coupled spins (condition 1), the magnetization of methyl protons reaches a maximum at time *n*/*J*, which is different from *TE*, when the lipid signal is strongest. The intensity of the lipid signal before and after *TE* decreases rapidly because of its large spectral bandwidth (0.9-1.4 ppm). Condition 2 means that the lipid signal is small when the lactate signal reaches its maximum. The separation between *TE* and *n*/*J* increases, the lipid signal decreases. However, increased separation also decreases the lactate signal because of the inhomogeneity of the static magnetic field. Therefore, optimization of the separation is the key of the proposed lactate-discriminating echo-shift technique. The echo-shift technique includes a modified data processing procedure to extract the lactate signal intensity from the reconstructed spectra (Fig. 2.4). First, a chemical shift region including the resonance of lactate methyl protons is selected.

This step removes the water signal and the signals of all other metabolites except lactate and lipid. The selected data are then translated into the pseudo-time-domain data by Fourier transformation. Finally, the signal intensity at n/J is calculated.

In practice, the maximum of the lactate signal becomes different from n/J because the inhomogeneity of the static magnetic field disturbs refocusing of the signal when TE is set apart from n/J. Therefore to obtain a better signal-to-noise ratio (SNR), the time at which the lactate signal is estimated should be changed from n/J. The time when the lactate signal was estimated and the separation between TE and n/J are shown in the section 2.3 Results and Discussion. The inhomogeneity also affects the intensity of the discriminated lactate signal, which can be corrected for by using the decay of an N-acetylaspartate (NAA) signal. The correction consists of the following steps: (step 1) select a chemical shift region including the resonance of NAA and translate the selected data into the pseudo-time-domain data by Fourier transformation; (step 2) calculate the ratio between the signal intensities at TE and the time at which the lactate signal was measured in the pseudo-time-domain data; and (step 3) divide the discriminated lactate signal intensity by the calculated correction ratio.

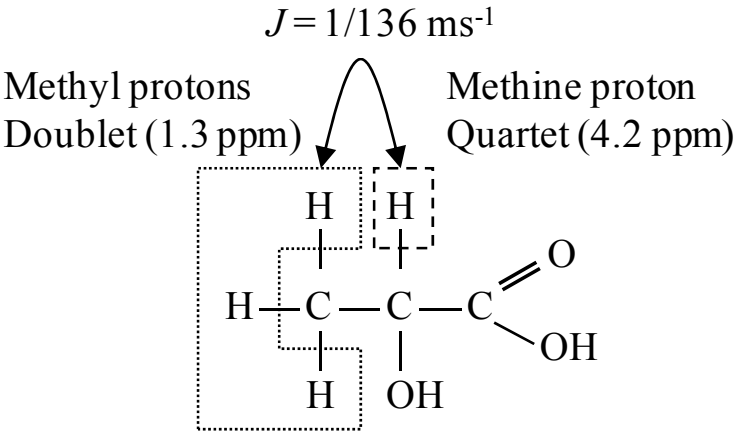

Figure 2.2. A schematic diagram of lactate molecule. Methyl protons and methine proton have *J*-coupling. Methine proton signal is difficult to be identified under large overlapped water signal. Methyl protons signal should be discriminated from overlapped lipid signal.

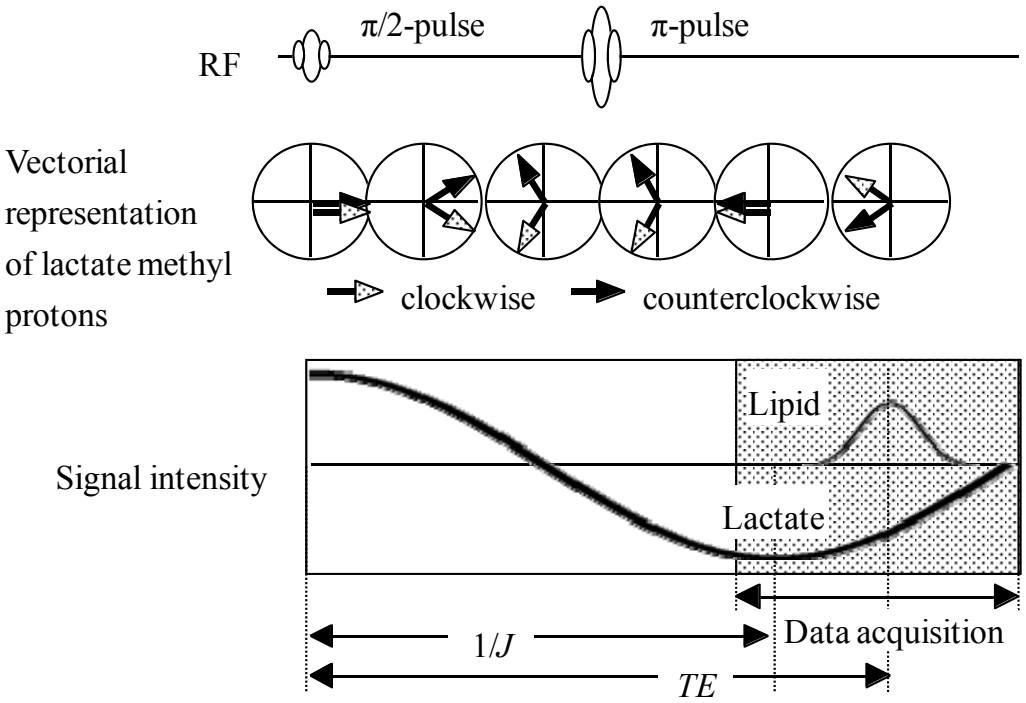

Figure 2.3. Illustration of the proposed lactate-discriminating technique. By using spin-echo technique, the signal intensity of the lactate methyl protons is strongest at time n/J due to J-coupling with the methine proton under ideal situation. The lipid signal is strongest at time TE and decreases rapidly because of its large spectral bandwidth.

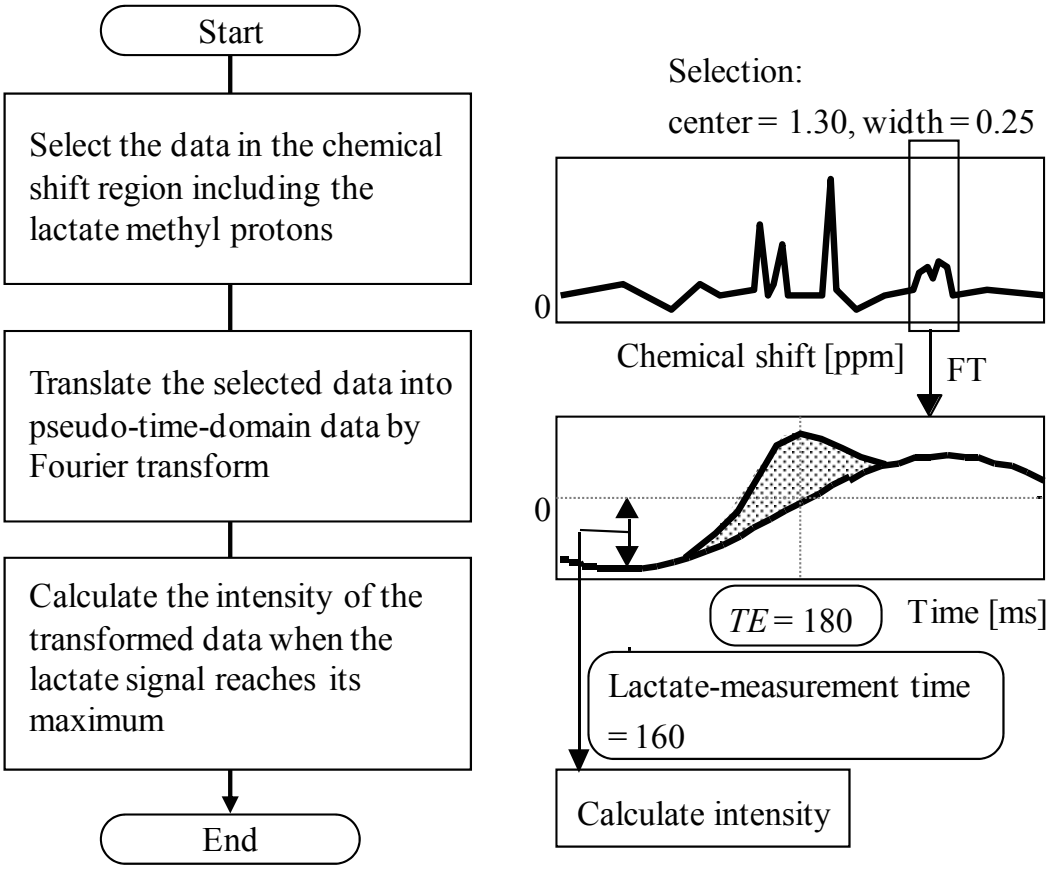

Figure 2.4. Algorithm of the proposed lactate-discriminating data processing. The lactate-measurement time is determined according to the separation between n/J and TE and the inhomogeneity of the static magnetic field. The lipid signal (shaded) is decreased at the time at which the lactate signal intensity is measured.

2.2.3 LACTATE-DISCRIMINATING ECHO-PLANAR SPECTROSCOPIC IMAGING TECHNIQUE

A schematic sequence diagram of the lactate-discriminating EPSI technique is shown in Fig. 2.5. The lactate discriminating EPSI technique needs spin-echo technique for combining the proposed lactate-discriminating echo-shift technique although the conventional EPSI technique does not need the spin-echo technique (Fig. 2.1). The measurement parameters were set to satisfy (condition 1) and (condition 2) with *TE* set at 180 ms, which differs from 1/*J* by 44 ms, and the lactate-measurement time was set at 160 ms, i.e. 20 ms earlier than *TE*. The validities of the selected *TE* and the lactate-measurement time are discussed in the section 2.3 Results and Discussion. As same as the conventional EPSI technique, an oscillating gradient was used to encode spectral and one-dimensional spatial information in the x-direction, and phase-encoding was used to obtain the spatial information in the y-direction. To improve the quality of acquired spectroscopic image, chemical shift selective (CHESS) pulse for water suppression [42] and outer volume suppression (OVS) pulse for subcutaneous fat suppression [43] were added before applying the π/2-pulse. The setting of these pulses was adjusted according to target objects.

Acquired data was reconstructed with correction of echo-planar trajectory as described in the section 2.2.1 Echo-planar Spectroscopic Imaging Technique. The lactate-discriminating data processing was applied in each pixel of the reconstructed spectroscopic image. The correction of the static magnetic field inhomogeneity was also applied in each pixel. In this calculation, the correction ratios used in (step 2) are smoothed along the spatial direction.

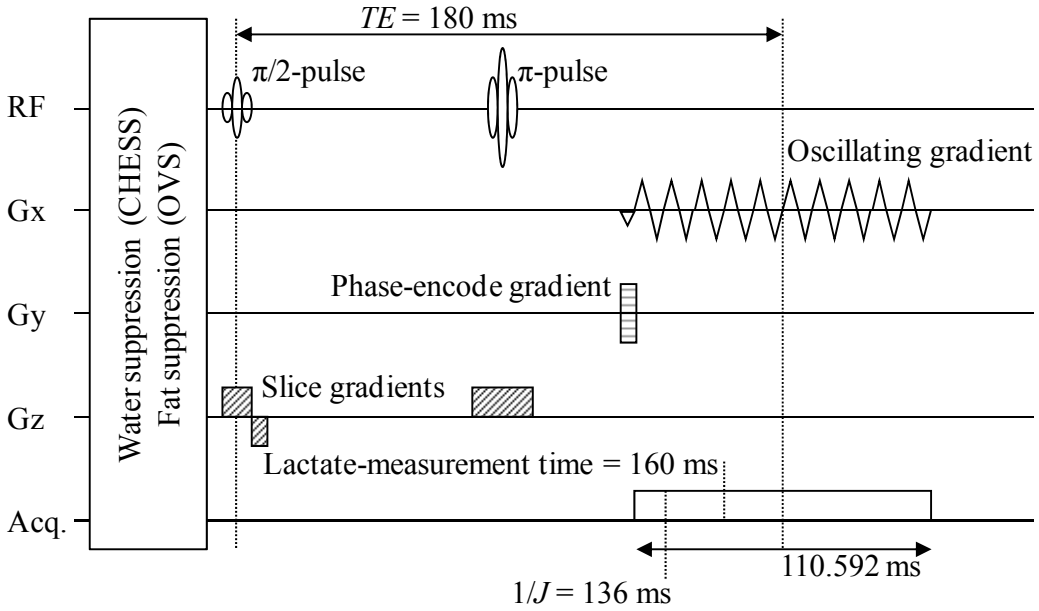

Figure 2.5. A sequence diagram of the proposed lactate-discriminating echo-planar spectroscopic imaging technique. This technique combines the proposed lactate-discriminating echo-shift technique with a conventional echo-planar spectroscopic imaging technique. The key of echo-shift technique is the setting of *TE* to sufficiently suppress lipid signal while maintaining lactate signal at lactate measurement time which is close to n/J.

2.2.4 EXPERIMENTS: CEREBRAL ISCHEMIA MODEL RATS

Experiments were performed using a 4.7-T MRI system for small animal study. It was equipped with actively shielded gradient coils that can produce 75 mT/m within 200 μs. An 8-element birdcage coil 4 cm in diameter and 4 cm long was used for both RF transmission and signal reception.

Seven focal cerebral ischemia models using male Sprague-Dawley rats, each weighing about 280 g, were measured. The rat was anesthetized with pentobarbital and urethane, and a femoral vein was cannulated for monitoring arterial blood pressure and acquiring samples for blood gas measurements. The blood samples were obtained at the intervals of the magnetic resonance measurements. Mechanical ventilation with a mixture of room air and O_2 gas was used in order to maintain blood gas levels within the normal ranges. The rectal temperature was maintained between 36.5°C and 37.5°C by using a warm water blanket. Focal cerebral ischemia in the right hemisphere was induced by tandem occlusion using intraluminal occlusion of the right middle cerebral artery and ligation of right common carotid artery [3]. The head of the rat was fixed to a bed with tape and inserted into the birdcage coil immediately after the surgery.

To compare the reduction of apparent diffusion coefficient (ADC) of water, which is a current standard to diagnose acute ischemic lesion, and the elevation of lactate concentration, two types of magnetic resonance measurements were used: (a) diffusion-weighted echo-planar-imaging (DW-EPI) technique and (b) presented lactate-discriminating EPSI technique. The DW-EPI was used to obtain a water ADC image [44, 45]. The DW-EPI used single shot and asymmetric spin-echo EPI, with *TR*/*TE* = 3000/90 ms, a field of view (FOV) of 40 × 40 mm (64 × 64 voxels), and a slice

thickness of 5 mm. OVS was applied to reduce artifacts from regions outside of the brain, especially from the subcutaneous fat. Seven *b*-values (0, 902, and 1409 $\times 10^6$ s/m^2 in each x-, y- and z-direction) were used to calculate the average water ADC [46, 47]. The lactate-discriminating EPSI technique was used to obtain metabolite images. For the EPSI acquisition, a 128-cycle sinusoidal oscillating gradient was used with an amplitude of 32.6 mT/m, a cycle time of 0.864 ms, and the signal was sampled 96 points per cycle. These parameters were set at a spectral bandwidth of 5.786 ppm, a FOV of 40 × 40 mm, and a slice thickness of 5 mm. The *TE* was set at 180 ms, which was separated by 44 ms from 1/*J*. Phase-encoding was applied with 15 steps, symmetrically distributed about the zero encode. The symmetry is necessary because an asymmetric encode leads to unwanted phase cycling in the reconstructed image. Water suppression was obtained by using three consecutive CHESS pulses and fat suppression was obtained by using eight OVS slices, applied prior to the $\pi/2$-pulse. The OVS slices were set apart from the brain in order to not reduce the signals of metabolites in the brain. For a *TR* of 4 seconds, 15 encodes, and 16 accumulations, the total measurement time was 16 minutes. Reconstruction was done similar as for conventional EPSI with the following steps: (step 1) divide the measured data into the even echoes and the odd echoes; (step 2) correct each of the two data sets for non-linear sampling due to measurement in the presence of the sinusoidal oscillating gradient; (step 3) fill zero-valued data to double the number of data in each chemical shift, x-direction and y-direction; (step 4) inverse fast Fourier transform; (step 5) apply zero- and first-order phase-correction, and chemical shift correction; and (step 6) add the two spectroscopic images obtained from the even echoes and the odd echoes [40]. This reconstruction used to provide the images of all metabolites except a lactate. To obtain the lactate image, the reconstructed data were processed by the

lactate-discriminating data processing procedure. The center of the selected chemical shift region was at 1.30 ppm and the region had a width of 0.25 ppm, and the lactate-measurement time used was 160 ms. In addition, the static magnetic field inhomogeneity correction using the NAA signal was applied. The DW-EPI and the lactate-discriminating EPSI were sequentially repeated three times in order to obtain a time series of the water ADC images and the lactate images. Shimming of the static magnetic field was done prior to each lactate-discriminating EPSI measurement.

2.3 RESULTS

Figure 2.6 shows a preprocessed spectroscopic image obtained by using the lactate-discriminating EPSI technique. Lipid signals were especially evident in two regions near the upper edge of the brain, that were too close to the brain to be suppressed by OVS. Imperfect excitation profile of OVS pulse may deteriorate the signal inside the brain if OVS is set too close to the brain. Contamination by these lipid signals made the lactate concentration indistinct in the upper right region of the brain. This was because the lactate signal was eliminated by the lipid signal, which has the opposite polarity. In the processed lactate image (Fig. 2.7), however, the lipid signal is suppressed and the region over which the lactate was increased can be clearly distinguished. Figure 2.8 shows the time series for the water ADC images and the lactate images. A strong correlation between the increase of lactate concentration and the decrease of water ADC can be seen, similar to that observed in previous reports [48–52]. The shortage of the oxygen and glucose supply after the onset of MCAO causes the tissue to switch to anaerobic

metabolism, leading to the increased lactate concentration. It has been reported that the energy failure due to this shortage leads to the decrease of ADC [48–52].

Figure 2.8 demonstrates the feasibility of getting a time series of the lactate images and the NAA images by this technique. It clearly shows the increased lactate concentration and stable NAA concentration through time. But, it also indicates a disadvantage of this technique. Although the lipid signal was sufficiently suppressed in the second and third lactate images, it is not sufficiently suppressed in the first image. The insufficient lipid suppression may be caused by the inhomogeneity of the static magnetic field. A large inhomogeneity shifts the lipid spectrum to the edge of the region that is selected in the lactate-discriminating data processing, which leads to an apparent narrowing of the lipid spectrum, and thus the lipid signal is not sufficiently decreased at the lactate-measurement time. The change of the inhomogeneity with time may have been the result of shimming before each measurement, instability of the static magnetic field, or a small movement of the rat head. This technique seems to have an advantage with regard to motion because it requires only a single measurement for lactate discrimination. But if motion induces a larger inhomogeneity, the lactate signal may not be sufficiently discriminated. Another disadvantage of the technique is that it requires a long echo time, which makes it hard to acquire metabolite signals having very short T_2 values. Finally, although setting $TE = (n+1/2)/J$ ensures that the measured value at TE comes only from the lipid signal, it results in a reduced lactate signal intensity.

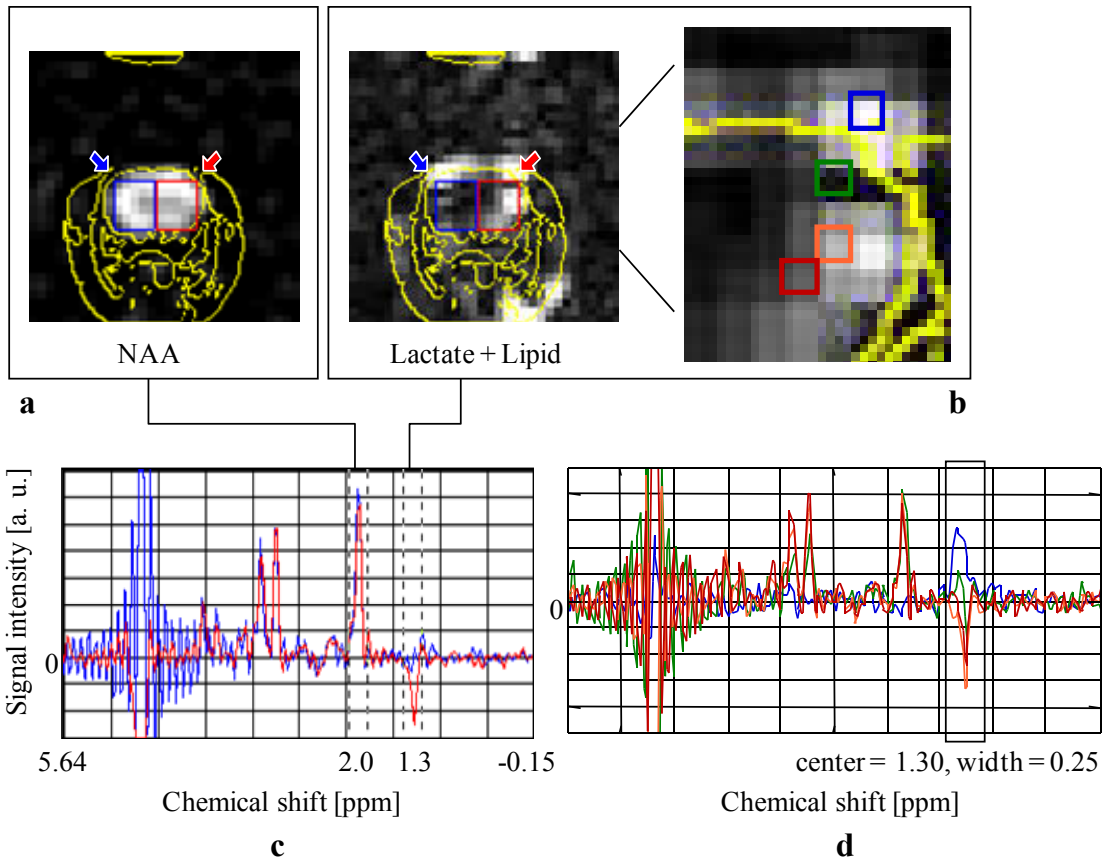

Figure 2.6. A spectroscopic image obtained without application of the lactate-discriminating procedure. The graphs (**c**, **d**) represent the spectra obtained from the rectangles drawn with the same colors. The images (**a**, **b**) were calculated by integrating the signal intensity in the selected chemical shift regions and taking their absolute values. The yellow lines represent the calculated outlines of an SE image. The right image of (**b**) is an enlarged image of the right hemisphere. The lactate signal intensity has a negative polarity because *TE* = 180 ms. Thus, around the edge of the right hemisphere (green rectangle) the contamination of the lipid signal makes the signal intensity lower than the actual value.

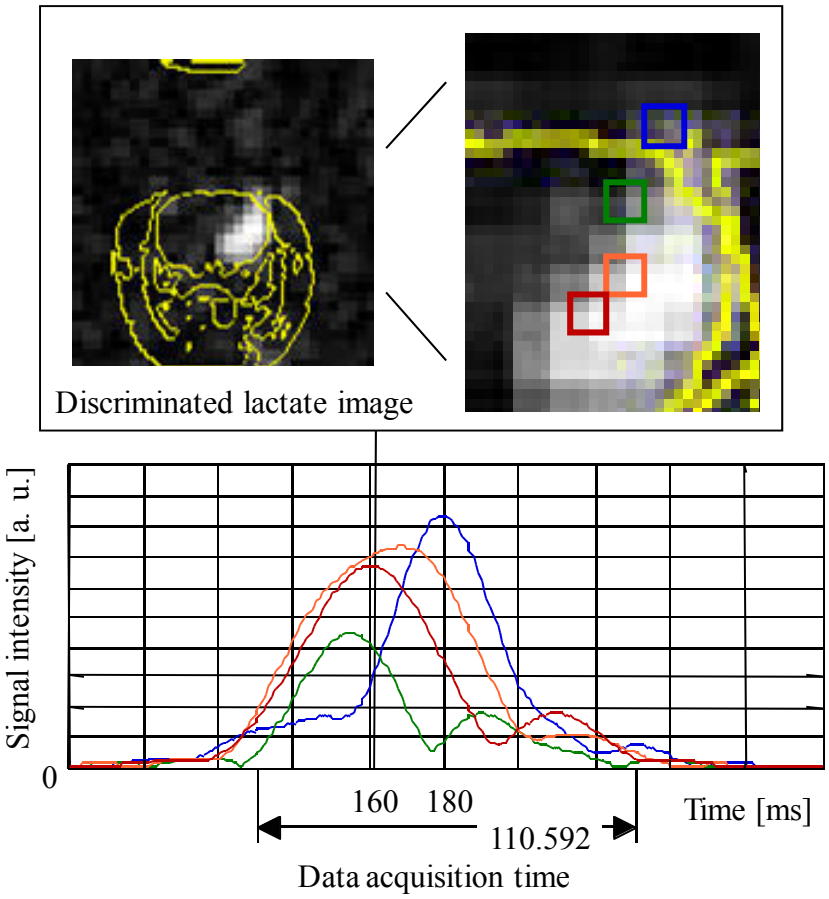

Figure 2.7. A processed lactate image obtained by the lactate-discriminating EPSI from the same data as shown in Fig. 2.6. The graph represents the pseudo-time-domain data obtained from the rectangles drawn with the same colors. The suppression of the lipid signal can be seen in the processed lactate image.

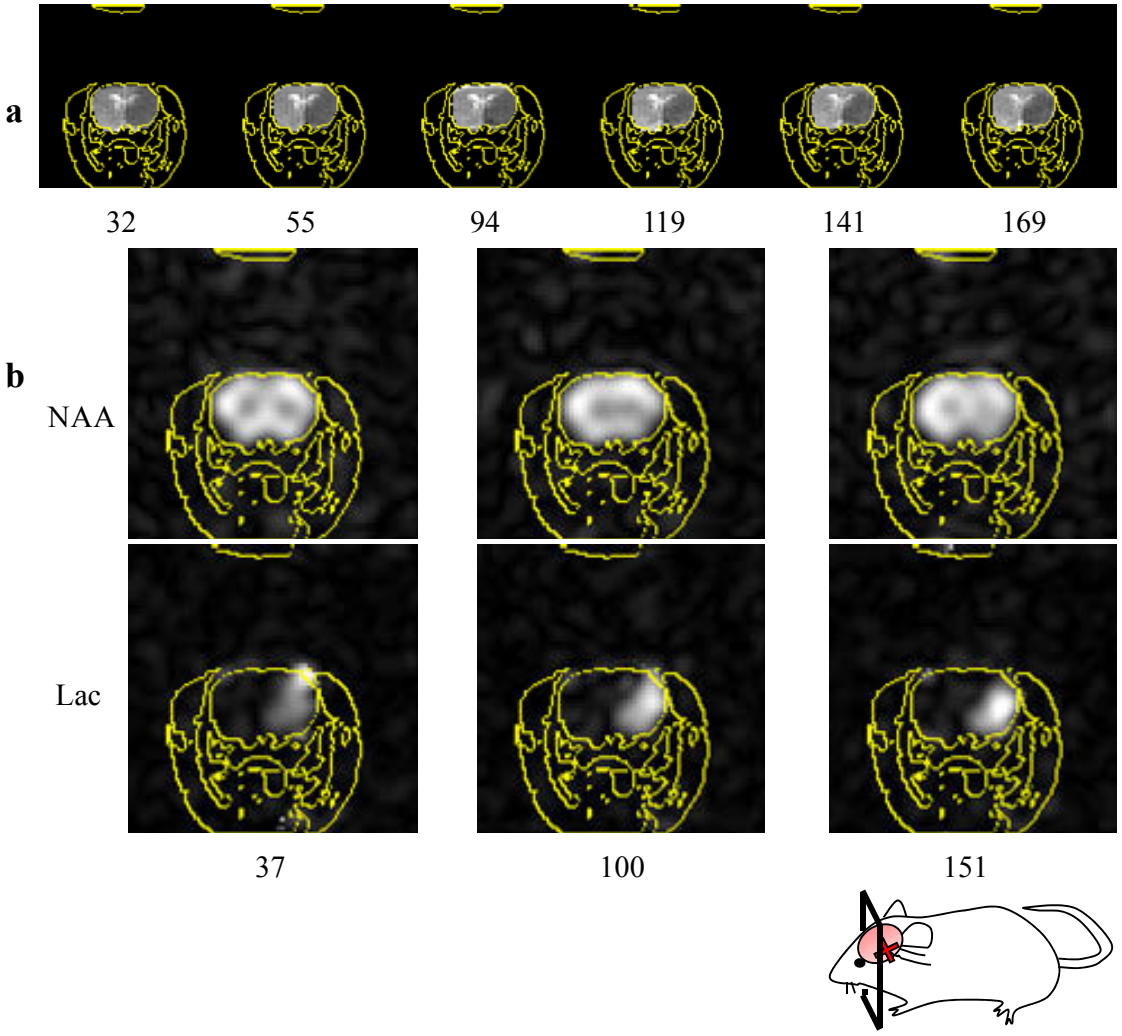

Figure 2.8. Images of a rat focal cerebral ischemia model: (**a**) a time series of the water ADC images obtained by the DW-EPI, and (**b**) time series of the NAA and lactate images obtained by the lactate-discriminating EPSI. The number under each image represents the time in minutes after the occlusion. The lactate concentration increases gradually through the time.

2.4 DISCUSSION

2.4.1 VALIDATION WITH COMPUTER SIMULATION

A computer simulation was used to estimate the suppression of the lipid signal and the lactate-measurement time needed for getting a better SNR. If we assume that the static magnetic field inhomogeneity can be represented by a Gaussian function, the lactate signal intensity $S_{\mathrm{Lac}}(t)$ can be described by the following equation:

$$S_{\mathrm{Lac}}(t) = S_{\mathrm{Lac}}(0) \cdot \cos\left(\frac{\pi t}{J}\right) \cdot \exp\left(-\frac{t}{T_{2,Lac}}\right) \cdot \exp\left(-\frac{(t-TE)^2}{2} \frac{\pi^2}{2\log(2)} \left(\frac{\gamma B_0}{2\pi}\right)^2 \sigma^2\right), \quad [2.1]$$

where t [s] is the time from π/2-pulse, $T_{2,\mathrm{Lac}}$ [s] is the T_2 of lactate, γ [radian/(s·T)] is a gyromagnetic ratio, B_0 [T] is the static magnetic field strength, and σ [ppm] is the half-power width of the inhomogeneity of the static magnetic field. The pseudo-time-domain data of lactate obtained by the lactate-discriminating data processing is approximated by $S_{\mathrm{Lac}}(t)$ because the spectral region is selected wide enough to include the lactate spectrum. If we assume that the shape of the lipid spectrum can be represented by a Gaussian function, the lipid signal intensity $S_{\mathrm{Lip}}(t)$ can be described by the following equation:

$$S_{\mathrm{Lip}}(t) = S_{\mathrm{Lip}}(0) \cdot \exp\left(-\frac{t}{T_{2,\mathrm{Lip}}}\right) \cdot \exp\left(-\frac{(t-TE)^2}{2} \frac{\pi^2}{2\log(2)} \left(\frac{\gamma B_0}{2\pi}\right)^2 \left(\sigma^2 + w^2\right)\right), \quad [2.2]$$

where w [ppm] is the half-power width of the lipid spectrum, and $T_{2,\mathrm{Lip}}$ [seconds] is the T_2 of lipid. The pseudo-time-domain data $S'_{\mathrm{Lip}}(t)$ of lipid obtained by the lactate-discriminated data processing can be represented by the following equation:

$$S'_{\mathrm{Lip}}(t) = S_{\mathrm{Lip}} \otimes R_u(t),$$
$$R_u(t) = \frac{\sin(\gamma H_0 u t/2)}{\pi t}, \qquad [2.3]$$

where $\otimes$ means convolution, and u [ppm] is the width of the selected chemical shift region used in the data processing. These equations can be used to determine the lactate-measurement time and TE, and to estimate the lipid suppression. In determining these times, it was required that the difference of these two values was 20 ms to suppress the lipid signal, and the lactate signal was strongest at the lactate-measurement time. The difference between TE and the time when the lactate signal is strongest increases as TE increases from $1/J$. The minimum TE that satisfies these constraints is 180 ms for a static magnetic field inhomogeneity of 0.05 ppm according to Eq. [2.1].

Figure 2.9 shows the calculated intensities of the lactate signal and lipid signal. In this calculation, it was assumed that the measurement and data processing were done as described in the section 2.2.4 Experiments: B_0 = 4.7 T, TE = 180 ms, and the selected chemical shift region used in lactate-discriminating data processing had its center at 1.3 ppm and had a width of 0.25 ppm. It was also assumed that the half-power width of lipid spectrum was 0.25 ppm and a static magnetic field inhomogeneity was 0.05 ppm. The calculated data fits well with the experimental data shown in Fig. 2.9. The lactate signal reaches its maximum near 160 ms. The estimated suppression of the lipid signal around this time is only about 10%, which is less than the measured suppression value, which from Fig. 2.7, was found to be about 30%. There are three possible explanations for this

as follows: (1) the data include the contamination of the lactate signal, (2) the magnetic field inhomogeneity is larger than the value assumed for the simulation, and/or (3) the shape of the lipid time-domain signal is far from Gaussian. The suppression may not be sufficient if the lipid signal is many times stronger than the lactate signal. An additional technique, such as OVS used in this experiment, may then be required. Equations [2.1] and [2.2] also point out that a greater static magnetic field strength and a more homogeneous static magnetic field may be required in order to improve the suppression of lipid signal and the SNR of the lactate image. According to Eq. [2.1], the smaller half-power width of the static magnetic field inhomogeneity can increase $S_{Lac}(t)$. The suppression of the lipid signal relative to the lactate signal is estimated by calculating $S_{Lip}(t)/S_{Lac}(t)$. According to Eqs. [2.1] and [2.2], the B_0-dependent part of $S_{Lip}(t)/S_{Lac}(t)$ is the last exponential term of Eq. [2.2], which represents the decay of the lipid signal due to its spectral bandwidth. The greater static magnetic field strength can narrow this part. For example, the lactate-measurement time and *TE* should be separated by more than 18 ms to suppress the lipid signal down to 10% if $B_0 = 4.7$ T, while they should be separated by more than 42 ms if $B_0 = 2.0$ T.

The time at lipid peak was estimated and used as the lactate measurement time in this development, but instead, the n/J can be simply used as the lactate measurement time although the intensity of lactate signal was decreased slightly. This simple modification has an advantage that lactate measurement time is independent from the inhomogeneity of static magnetic field. Preliminary result using this simple modification of this technique was reported about optimum TE for various static magnetic field strength [53]. The optimum *TE* was 165 ms (i.e. separation was about 25

ms) at 7 T, 180 ms (i.e. separation was about 40 ms) at 4.7 T, and 200 ms (i.e. separation was about 60 ms) at 3 T.

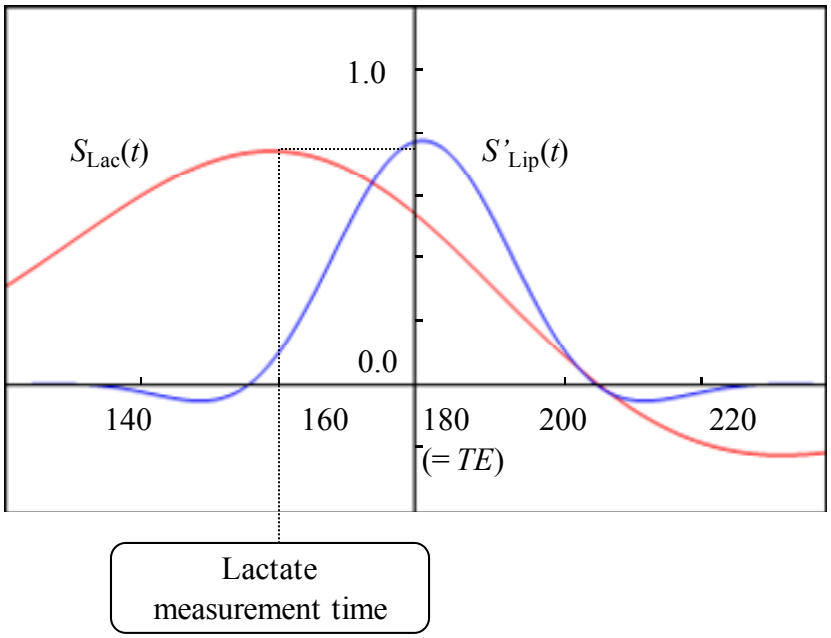

Figure 2.9. The lactate signal ($S_{Lac}(t)$) and lipid signal ($S'_{Lip}(t)$) calculated by computer simulation. The sign of $S_{Lac}(t)$ was inverted to clearly show the peak amplitude. The calculated signal intensities fit well with the experimental data.

2.4.2 TECHNOLOGY IMPROVEMENTS

Lactate-discriminating echo-shift technique can be taken as a special line-profile selection in two-dimensional spectroscopy which is usually used to analyze structure of molecule in NMR. The two-dimensional spectroscopy acquires data while changing *TE* and applies Fourier Transform also in the direction of *TE*. It can discriminate lactate more precisely from lipid; however, it takes a long measurement time to acquire data with various *TEs*. The proposed lactate-discriminating echo-shift technique is to find and use the line-profile at special *TE*.

Further improvements of the technique are possible. For example, the lactate discriminating echo-shift technique can be combined with other fast MRSI techniques such as projection-reconstruction echo-planar technique [54], multiple spin-echo spectroscopic imaging [55], spiral spectroscopic imaging [56], steady-state free precession spectroscopic imaging [57], parallel spectroscopic imaging [58], and compressed sensing spectroscopic imaging [59]. Further improvement will be possible by introducing fast imaging technique for basic MRI including multiband excitation technique and spatial localization excitation technique. These techniques can be used to decrease the measurement time as well as to increase the spatial dimension. The multiple spin-echo spectroscopic imaging can be used to improve accuracy of discriminating lactate because it can acquire two-dimensional spectral information when appropriate *TEs* are selected.

The inhomogeneity correction using the NAA signal can be modified to use the water signal. The NAA signal is not a good reference because NAA is found mostly only in nervous tissues and is decreased by some diseases. The use of a water reference might

avoid this problem, for which the EPSI technique will be particularly useful because it reduces the amount of time required for the measurement.

The lactate-discriminating data processing can be modified to calculate the intensity of the lactate signal by curve fitting. This may increase the SNR of the resultant lactate image because the intensity would then be calculated by using several points instead of only one point. The measurement parameters might also be changed to acquire a better SNR of the lactate image, by setting the lactate-measurement time to $1/J$, and by setting TE closer to the $1/J$ value than that was used in this study. The measurement parameters might also be changed to use a more recent measurement of the lactate J-coupling constant, which indicates that the actual value of $1/J$ is 145 ms [60], whereas in this experiment and simulation we have assumed it to be 136 ms.

The measurements of lactate-discriminating EPSI technique can also be modified to acquire more detailed information through time. In this experiment, the signal averaging was completed at each phase-encoding step, and the zero-encoded data were obtained at the beginning of each measurement. Thus the lactate image obtained was considered to largely reflect the concentration at the beginning of the measurement. However, if the order of the signal averaging and phase-encoding steps are interchanged, then the lactate image reflects the average lactate concentration during the measurement time. Furthermore, a lactate image could be obtained for each signal average. In this case, although the time-resolution of the lactate images would be improved, the SNR of each image would be decreased. Calculations of a moving average may be useful in obtaining a reasonable time-resolution and SNR.

Although only the signal intensity of lactate was estimated in this thesis, the concentration of lactate can be quantified by comparing with the other reference molecule. Most useful reference molecule is water, of which concentration is about 55 M in normal tissue [61]. The concentration of lactate can be quantified by calculating the signal ratio to the water signal acquired without water suppression. Further correction techniques about T_2 and T_1 may be necessary for improving accuracy of the quantified lactate concentration.

2.4.3 APPLICATION EXPANSION

The precise time-series analysis between lactate distribution and water ADC map by using the developed lactate-discriminating EPSI was reported for the focal cerebral ischemia model rats [62]. The result showed that elevated lactate concentration and normal water ADC were observed in the surrounding area of ischemia at 20 minutes after onset of ischemia. In the surrounding area, lactate concentration was elevated and the water ADC was progressively decreased to abnormal level. It suggests that the mismatch between increase of lactate concentration and decrease of water ADC may be a potential indicator to identify ischemic penumbra.

The remote MCAO technique will be useful for this study using rat models [63]. The remote MCAO enables arterial occlusion to be controlled from outside the MRI system while the rat is in the system. This technique has two advantages: it allows the static magnetic field homogeneity to be improved because the shimming of the magnetic

field can be done thoroughly before the occlusion, and it allows measurements to be made soon after the onset of occlusion and reperfusion.

This technique will be applied for investigation of other diseases than stroke. For example, this technique can be applied to detect hypoxic region in cancer by lactate elevation, which is important for radiation therapy, because hypoxic region has more radiation resistance.

2.5 CONCLUSION

A fast lactate-discriminating technique for ^{1}H spectroscopic imaging, which is a combination of lactate-discriminating echo-shift technique and conventional EPSI technique, has been developed. This technique has been used to measure a time series of lactate distribution in rat focal cerebral ischemia models. The results demonstrate the efficiency of discriminating the lactate signal from the lipid signal and the capability of acquiring spectra of other metabolites. They indicate that this technique needs a long *TE* and supplementary lipid suppression technique. They also indicate that the discriminated lactate image can be improved by ensuring that the static magnetic field is more homogeneous. This lactate-discriminating EPSI will be useful for dynamic anaerobic metabolism observing fast changes of the concentrations of lactate and other metabolites.

CHAPTER 3 FAST DIFFUSION-WEIGHTED SPECTROSCOPIC IMAGING TECHNIQUE TO MEASURE MOLECULAR DIFFUSION

3.1 INTRODUCTION

Measurements of molecular diffusion may provide useful information about cell or tissue structures and functions because diffusion coefficients are related to compartmentation, membrane permeability, transport processes, and temperature [64-66]. Since diffusion imaging of water was developed *in vivo* [67, 68], valuable information has been made available about brain diseases such as stroke, cancer, and neurologic disorders. Recently, techniques for high-speed diffusion imaging have been investigated [44, 45], making course-of-time studies [69] as well as abdominal studies [70] possible. Most research has been performed on water; however, it may not be the most suitable molecule for observing cell or tissue structures and functions because water does not sufficiently reflect their features. In fact, water is not obstructed much by most membranes and water exists both intra- and extra-cellular spaces.

In order to obtain local transport of metabolites, some works have been performed on other molecules than water by localized spectroscopy. ^{31}P diffusion-weighted spectroscopy has made it possible to obtain diffusion coefficients of adenosine triphosphate (ATP), phosphocreatine (PCr), and so on [5]. ^{1}H diffusion-weighted spectroscopy has made it possible to obtain the coefficients of N-acetylaspartate (NAA), choline-containing compounds (Cho), and so on [71-73]. To observe dynamic metabolism *in vivo*, diffusion-weighted spectroscopic imaging (DWSI) technique or

multi-voxel diffusion-weighted spectroscopy (DWS) technique is required. First report on DWSI technique only provides diffusion-weighted spectroscopic image, that enhances the effect of diffusion, but does not calculate the diffusion coefficient of spectroscopic image [74]. The reason is that the time required for measurement by this technique was so long, because it is based on three-dimensional chemical shift imaging (3D-CSI) technique which uses two-dimensional phase-encodings. Thus, the improvements in mapping the diffusion coefficient of spectroscopic image may not be easy under the restriction of measurement time. Furthermore, the longer measurement time will increase the possibility that motion artifacts occurs. The main disadvantages of diffusion-weighted spectroscopic imaging are probably a long measurement time, low signal-to-noise ratio (SNR) and motion artifacts *in vivo*.

In this chapter, high-speed DWSI technique is presented [20], which is based on the conventional echo-planar spectroscopic imaging (EPSI) technique. In it, a pair of diffusion gradients is provided prior to providing a rapidly oscillating gradient. The gradient is modified to encode both spectral information and spatial information of one direction [17, 18], in contrast with conventional echo-planar technique encoding spatial information of two directions [75]. It is validated using a phantom consisting of acetone and water. A diffusion-weighted spectroscopic image is obtained in about 15 minutes, which is estimated to be about 64 times faster than the conventional method based on 3D-CSI. The measured diffusion coefficients show good agreement with previously reported values.

3.2 MATERIALS AND METHODS

3.2.1 DIFFUSION-WEIGHTED ECHO-PLANAR SPECTROSCOPIC IMAGING TECHNIQUE

Figure 3.1 shows a schematic sequence diagram of the presented diffusion-weighted echo-planar spectroscopic imaging (DW-EPSI) technique. In order to add diffusion sensitivity, a pair of large diffusion gradients is inserted prior to adding the oscillating gradient. The amplitude of this pair of diffusion gradients is changed to alter the signal attenuation caused by molecular self-diffusion. When the amplitude of the diffusion gradients is fixed, the procedures for measurement and reconstruction are done in a way similar to the way they are done in EPSI technique, which is described in the section 2.2.1 Echo-planar Spectroscopic Imaging Technique. An apparent diffusion coefficient (ADC) is calculated in each corresponding pixel over the series of spectroscopic images according to the following equation:

$$\log(S(b)) = -Db + \log(S(0)), \qquad [3.1]$$

where S is signal intensity and b is a b-value (i.e. gradient factor) given by $b = \gamma^2 G^2 \delta^2 (\Delta - \delta/3)$, in which G, δ, and Δ denote the amplitude, duration, and separation of the diffusion gradients, respectively [64].

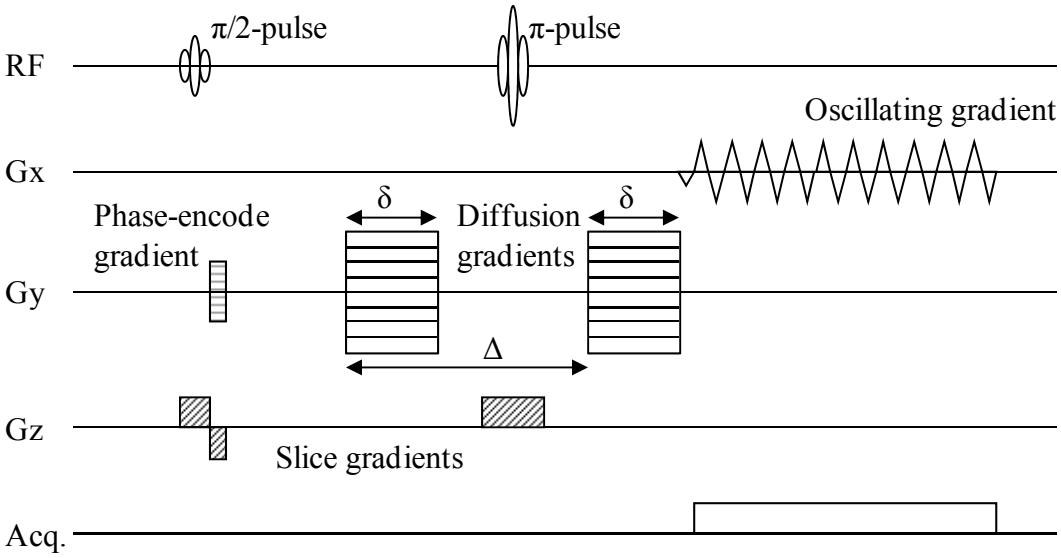

Figure 3.1. A sequence diagram of the proposed diffusion-weighted echo-planar spectroscopic imaging technique. A pair of diffusion gradients is inserted prior to providing the oscillating gradient in order to add diffusion sensitivity.

3.2.2 *EXPERIMENTS: PHANTOM OF TWO MATERIALS*

Experiments were performed using a prototype 4.7-T magnet equipped with 30-cm-bore actively shielded gradient coils, and an 8-cm-diameter birdcage coil, for RF transmission and signal reception, tuned to a resonant frequency of ^{1}H. The phantom used consisted of two 22-mm-diameter bottles, one filled with acetone and the other with water. The diffusion gradients were applied in the y-direction with amplitudes of 0, ±5, ±10, ±15 mT/m, a duration δ of 20 ms, and a separation Δ of 65 ms. The *b*-value *b* was up to 3.76×10^8 s/m^2, which sufficiently attenuated the water signal at about 1/2. The polarity of the two diffusion gradients was altered at each amplitude to reduce the effect on diffusion attenuation of the magnetic field inhomogeneity [76]. For other words, the alternations of the diffusion gradients reduce the effects on diffusion attenuation of any other gradients applied in the same direction [77]. In these experiments, however, no other gradients causing diffusion attenuation were applied in the same direction. The oscillating gradient was designed to have a 32-cycle sinusoidal shape with an amplitude *A* of 15 mT/m and cycle time *c* of 1.536 ms. The signal was sampled at 256 points per cycle. The sinusoidal shape was chosen to decrease the power needed to drive the gradient coil. Those parameters were set at a spectral bandwidth l_f of 6.4 ppm (1280 Hz), a field of view of 13 cm (double sampling), and a spatial resolution r_x of 3 mm. The relations are described by the following equation:

$$\begin{cases} l_f = \dfrac{4\pi}{\gamma H_0 c}, \\ r_x = \dfrac{2\pi^2}{\gamma A c}, \\ \dfrac{l_f{}^2}{r_x} = \dfrac{4P}{\gamma H_0{}^2}, \end{cases} \qquad [3.2]$$

where H_0 is the static magnetic field strength, and P is the slew rate given by $P = 2\pi A/c$. Because P is limited to less than about 60 T/m·s for the gradient unit, the spectral bandwidth and the spatial resolution are limited according to the last equation making up Eq. [3.2]. The compensating gradient which corresponds to a 1/4 cycle of the sine-oscillating gradient was applied before the oscillating gradient. The sine-oscillating gradient, compensating gradient, and data sampling timing were carefully adjusted to generate echoes at every peak of the sine-oscillating gradient. The sine-oscillating gradient has a negligible effect (less than 0.1%) on the calculated diffusion coefficients for those parameters, because the *b*-value of one cycle is no larger than 1.7×10^3 s/m^2. The amplitude of the phase-encode gradient was changed by 64 steps so that the field of view in the y-direction was 13 cm. Every spectroscopic image, when the amplitude of the diffusion gradients was fixed, was obtained with a slice thickness of 4 mm, a spectral width of 6.4 ppm, and a 13×13 cm^2 field of view. There were 64 pixels in the frequency-direction and 64 pixels in each spatial direction. At a *TR*/*TE* of 2000/120 ms and one accumulation, it took a total of about 15 minutes to measure a series of seven spectroscopic images. Temperature was kept 22°C throughout the experiments.

Reconstruction was done by Fast Fourier transform (FFT) in both the frequency- and y-directions, and by Fourier transform (FT) with sine-correction according to the following equation in the x-direction.

$$S(x) = \sum_{k_x=-N_x/2}^{N_x/2-1} \hat{S}(k_x) \cdot \exp\left(i\, x \sin\left(\frac{\pi k_x}{N_x} \right) \right) \cdot \cos\left(\frac{\pi k_x}{N_x} \right), \qquad [3.3]$$

where $\hat{S}(k_x)$ is the measured data along the x-direction, N_x is amount of data along the x-direction (a half of the sampling points per cycle), and i denotes an imaginary unit.

This equation is derived from Eq. [9] of Ref. [39]. The cosine part denotes the weighting factor of FT, which is reciprocal to the sampling point density. A summation was done for each image over each chemical shift area of both acetone and water, resulting in a total of two pixels in the frequency-direction. Because the objects consisted of only two kinds of molecules of which the spectra were not superposed, no severe spectral resolution technique was necessary. The diffusion-weighted spectroscopic image was calculated in each corresponding pixel over the series of images by the linear least-square method, according to Eq. [3.1].

To ease data handling, both the diffusion coefficient image and the signal intensity image were linearly interpolated, then the background was extracted by setting thresholds in the signal intensity image. Finally the corresponding background area of the diffusion coefficient image was filled with 0.

3.3 RESULTS

Figure 3.2 shows a spectroscopic image obtained by the proposed technique without diffusion gradients. It took about ten minutes per spectroscopic image for reconstruction with a workstation (56 MIPS) because the FT with sine-correction required a huge number of operations. However, calculating the value on a lattice by interpolation prior to FFT, instead of FT with sine-correction, may shorten the reconstruction time. In addition, there is an aliasing peak of water to the left of the acetone peak in Fig. 3.2c. The reasons for this are (1) the effects of the chemical shift are different between even and odd echoes, because the polarity of the oscillating

gradient is inverted, or (2) the echo times are miscentering because of eddy-current or timing-adjustment error. In either case, water was more strongly influenced because its chemical shift was further from the central frequency than that of acetone was. Applying some correction techniques in the frequency-direction may decrease this aliasing.

Figure 3.3 shows a diffusion-weighted spectroscopic image obtained by the proposed technique and its profile along the line drawn in the image. No clear artifact is apparent. Figure 3.4 shows the attenuation of signal intensity relative to the *b*-value *b* on pixels located in the middle of each bottle. The measured data shows good fits to Eq. [3.1]. In addition, the correlation coefficients appeared to be larger than 0.98 for all pixels except those in the background. Table 3.1 shows diffusion coefficients and standard deviations for circles with radii of 4 pixels located in the middle of each bottle. The measured diffusion coefficients show good agreement with previously reported values. This proves the validity of this technique.

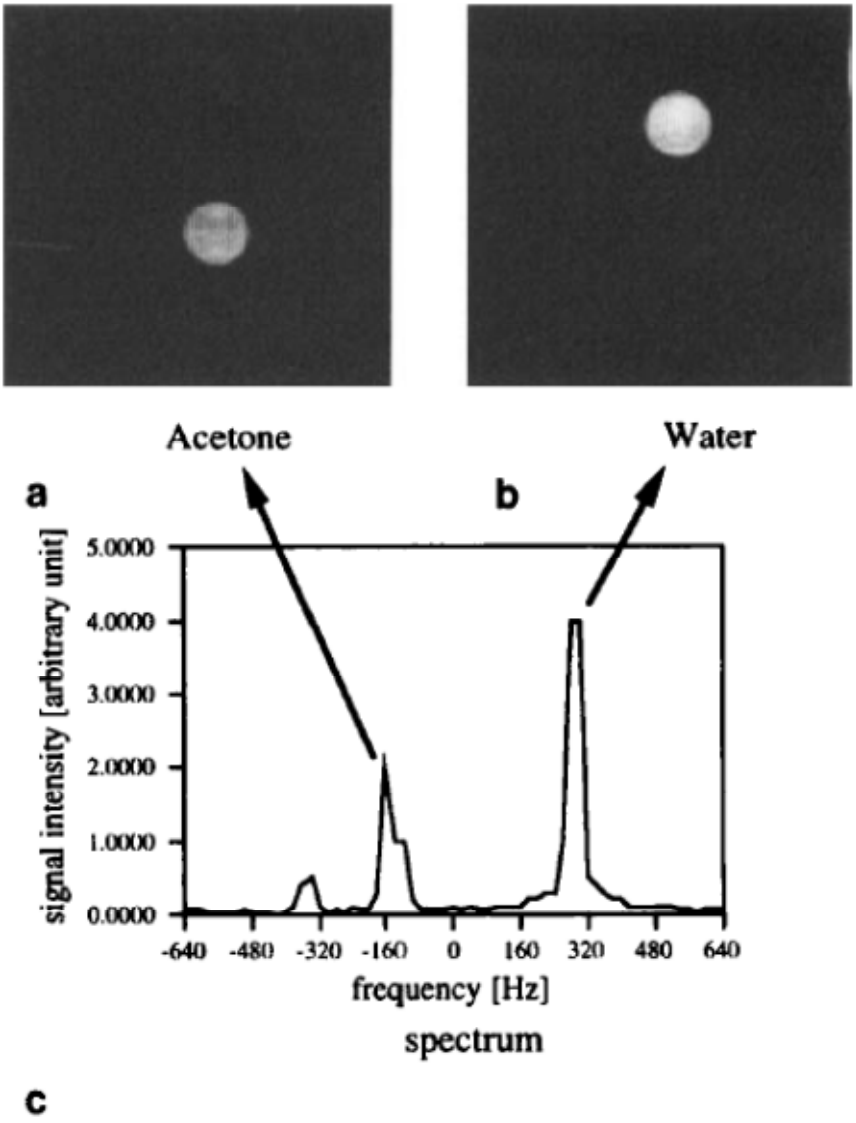

Figure 3.2. Spectroscopic image obtained by diffusion-weighted echo-planar spectroscopic imaging without diffusion gradients. (a) and (b) are intensity maps of acetone and water, respectively, with a field of view of 13 × 13 cm^2 and an original 64 × 64 pixels that are linearly interpolated to 128 × 128. (c) is the spectrum representing the summation over all spatial pixels.

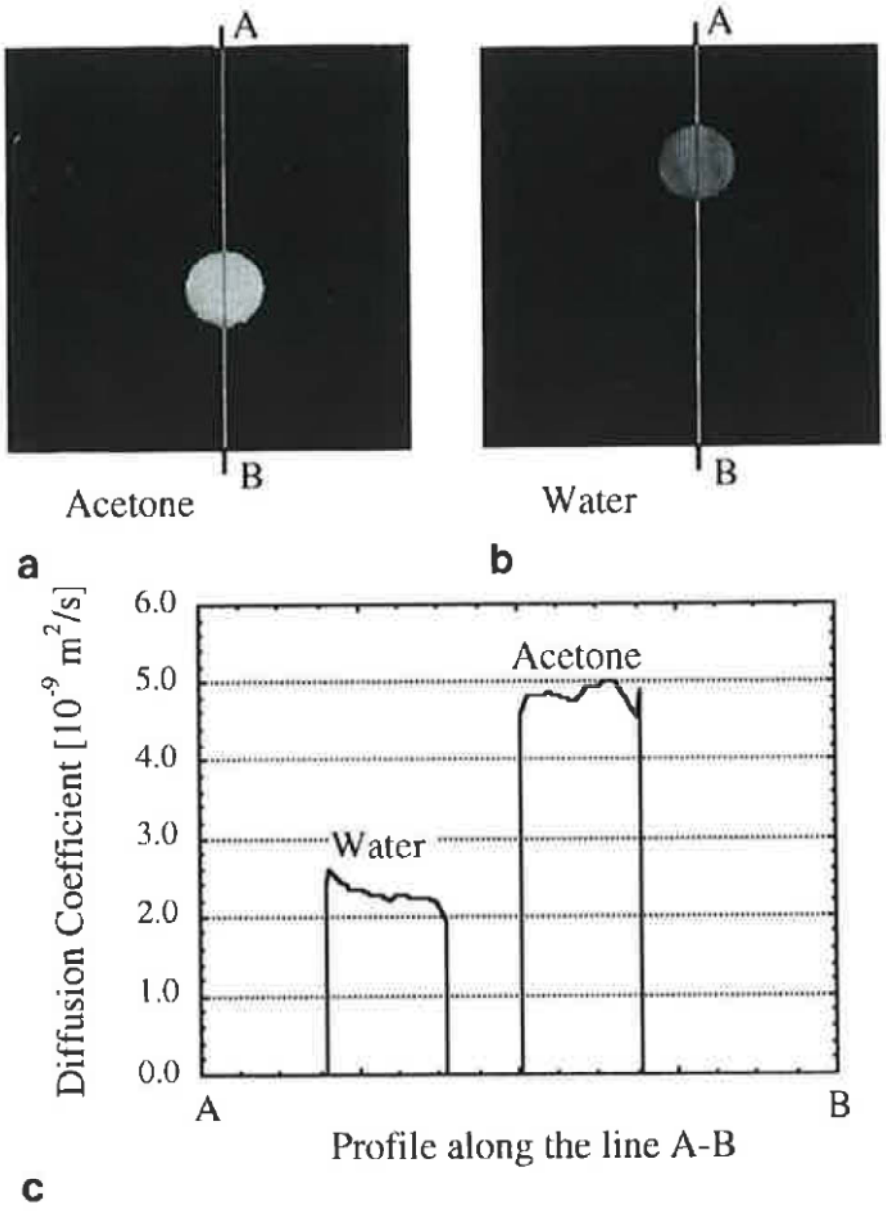

Figure 3.3. Diffusion-weighted spectroscopic image obtained by diffusion-weighted echo-planar spectroscopic imaging. (a) and (b) are diffusion coefficient maps of acetone and water, respectively, with a field of view of 13×13 cm^2 and an original 64×64 pixels that are linearly interpolated to 128×128. (c) is profiles of (a) and (b) along the line A-B.

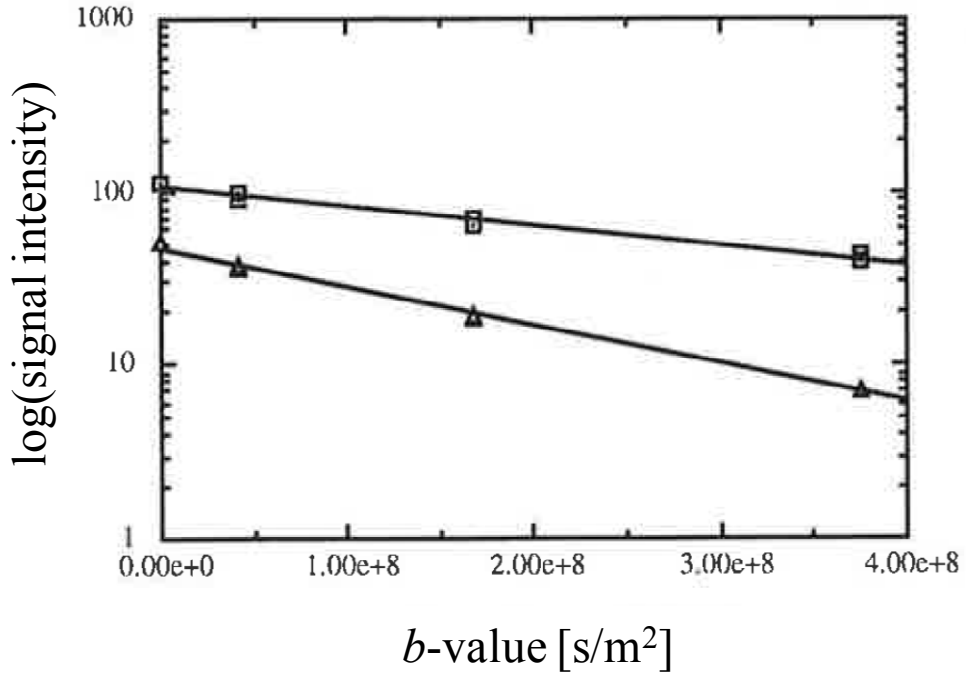

Figure 3.4. Half-logarithmic plot of the signal intensity versus the *b*-value. (□) and (△) denote acetone and water, respectively. Data were taken from points located in the middle of each bottle. The two lines are calculated fits to Eq. [3.1].

Table 3.1. Calculated ADC of NAA and water in a phantom and a rat brain by using DW-LSEPSI.

Material	Measured[a] values (10^{-9} m^2/s)	Reported[b] values (10^{-9} m^2/s)
Acetone	4.89 ± 0.06	4.97 ± 0.20
Water	2.22 ± 0.07	2.21 ± 0.10

[a] Diffusion coefficient maps are obtained from which these values are calculated in regions of interest at 22°C.

[b] Taken from Table 2 of Le Bihan D, et al., Radiology 1998;168:497-505. The temperature was 25°C. Thus, the diffusion coefficients and standard deviations cannot be compared directly because the temperatures and regions of interest are different.

If we suppose that the conventional DWSI based on 3D-CSI technique is applied, measurement is estimated to take about 950 minutes with 64 × 64 spatial pixels, a series of seven images, and *TR* of 2000 ms. This is because two-dimensional phase-encodings are necessary. Contrarily, the acquisition time of only 15 minutes using the proposed DW-EPSI technique is approximately 64 times faster than that of the conventional method. This is possible because one of the phase-encodings is replaced by the oscillating gradient. Although this improved speed is ideal because EPSI decreases SNR depending on the speed, DW-EPSI is useful in reducing the measurement time while balancing the obtainable SNR.

3.4 DISCUSSION

The proposed technique has potential for mapping the molecular diffusion coefficient of metabolites sequentially over time. In principle, only two spectroscopic images are necessary to calculate the diffusion coefficients. Furthermore, if we use antisymmetric pairs of bipolar shaped diffusion gradients, the alternations in the diffusion gradients are not necessary to reduce the effects of inhomogeneity [78]. The technique, however, requires more gradient amplitude because the interval of diffusion gradient is restricted. If we upgrade the gradient unit, the measurement time can be reduced. Another advantage of the technique is reduction of sensitivity to flow or macroscopic motion. The antisymmetric bipolar gradients desensitized the measurement to constant velocity flow and motion.

This powerful gradient unit has another advantage in improved spectral quality. In this experiment, there remained aliasing peak because both even and odd echoes were sine-corrected in the time-direction and Fourier transformed to obtain a spectroscopic image (Fig. 3.2c). However, the interval between even and odd echoes was changed and could not be fully corrected in the time-direction when k_x is not equal zero. If the frequency of the oscillating gradient can be double by using the powerful gradient unit, then another reconstruction technique can be used to remove such aliasing peak. The reconstruction technique divides even- and odd-echo data sets at first, separately applies sine-correction and Fourier transform to obtain even- and odd-echo spectroscopic images, and add acquired two spectroscopic images as shown in the section 2.2.4 Experiments. This modified reconstruction technique will remove the aliasing peak because the interval within each even- and odd-echo data sets is the same.

In this context, we have not treated non-proton nuclear, ex. ^{31}P, because this technique has a weakness with it. The main problem is related to the gradient unit, especially with regards to the maximum strength and the slew rate. In applying this technique to ^{31}P diffusion-weighted spectroscopic imaging using the same gradient unit, the spatial resolution was limited to no less than 18 mm, because the required observable spectral bandwidth must be no less than 30 ppm, according to Eq. [3.2]. Some techniques, however, have been investigated to deal with this problem [18, 79]. The powerful gradient unit has also applicable to solve this problem.

Further technical improvement of the proposed DW-EPSI technique is possible. For example, conventional water suppression technique and/or fat suppression technique can be combined with the proposed DW-EPSI to obtain metabolites diffusion

in vivo [40]. This preliminary report also shows that three-dimensional spatial information can be acquired by adding phase-encode gradient also in Gz. Although this technique has an advantage in acquiring three-dimensional spatial information with improved SNR, it is difficult to maintain homogeneity of static magnetic field in all region of interest. More detailed information about metabolites diffusion can be obtained. The direction of diffusion gradient can be changed to obtain diffusion tensor imaging (DTI) for each molecule [80]. This technique enables investigation on direction of microscopic transport of metabolites. Multiple *b*-values can be used to obtain property of non-Gaussian diffusion, similar to q-space imaging technique [81]. This technique enables investigation on microscopically inhomogeneous diffusion of metabolites.

A major issue for DWSI is to improve accuracy of acquired ADC under the restriction of SNR and the measurement time. An approach to address this issue is to calculate optimum *b*-values to maximize the accuracy of acquired ADC. Preliminary result has shown that optimum *b*-values are separated about 1/ADC for two *b*-value measurements [82]. It means that the optimum *b*-values for metabolite are much higher than that for water because the ADC of metabolite is much smaller than that of water. Higher *b*-values have some disadvantages, for example, they may cause large eddy-current distortions in the acquired images, and they may cause larger phase errors leading to motion artifacts during diffusion time, i.e. interval of the diffusion gradients. The fast measurement technique is useful to reduce motion artifacts caused by inter-sequence movements; however, there remains technical challenge to reduce motion artifacts caused by such intra-sequence movements. An approach to reduce motion artifacts will be discussed in the next chapter 4 Diffusion-weighted

Spectroscopic Imaging Technique to Reduce Motion Artifacts in Metabolites Diffusion Imaging.

3.5 CONCLUSION

High-speed diffusion-weighted spectroscopic imaging based on an echo-planar spectroscopic imaging technique was presented. A pair of diffusion gradients was applied prior to a rapidly oscillating magnetic field gradient which encodes both chemical shift and spatial information. By applying this technique to a phantom consisting of acetone and water, a diffusion-weighted spectroscopic image was obtained in about 15 min, about 64 times faster than the time required in the conventional method. The measured diffusion coefficients showed good agreement with previously reported values. This kind of diffusion-weighted spectroscopic imaging technique is expected to provide a way to observe microscopic dynamic metabolism.

CHAPTER 4 DIFFUSION-WEIGHTED SPECTROSCOPIC IMAGING TECHNIQUE TO REDUCE MOTION ARTIFACTS IN METABOLITES DIFFUSION IMAGING

4.1 INTRODUCTION

Metabolite diffusion is expected to provide useful information regarding cellular and tissue microstructures and functions, such as cell size, permeability, and intracellular transport [5, 71, 73, 83]. Many studies have used diffusion-weighted spectroscopy (DWS) especially to investigate changes in metabolite diffusion at ischemia [84-88] and properties of metabolite diffusion that differ from those of water [89-94]. However, only a few studies have employed diffusion-weighted spectroscopic imaging (DWSI) [74, 75, 20]. One reason is that an efficient measurement technique has not been developed to obtain highly accurate diffusion-weighted images (DWI) of metabolites. The issues in developing the technique are low signal-to-noise ratio (SNR), long measurement time, low spatial resolution, and artifacts caused by magnetic field inhomogeneity. However, the most challenging issue is to reduce motion artifacts caused by cardiac pulsation or respiration [75]. Such motion during diffusion time induces an imbalance of the diffusion gradients that causes phase errors. The phase errors become much larger when larger *b*-values are used for the accurate detection of diffusion of metabolites that is smaller than diffusion of water. The large phase errors hinder accurate phase-encoding and produce ghosting artifacts in imaging. Furthermore, they hinder accurate amplitude summation and cause significant signal loss artifact in signal averaging which is necessary to mitigate the low SNR of metabolite signals. These phase errors depend on spatial location and

vary with time, so they are significantly difficult to correct using conventional phase-encoding. Thus, such motion artifacts have not been effectively reduced using proposed diffusion-weighted chemical-shift imaging with two-dimensional phase-encoding and navigator echo [95] and diffusion-weighted echo-planar spectroscopic imaging (DW-EPSI) that uses echo-planar and one-dimensional phase-encoding [20]. Diffusion-weighted line-scan echo-planar spectroscopic imaging (DW-LSEPSI), which uses echo-planar and line-scan techniques instead of phase-encoding, has been proposed to reduce such motion artifacts and tested by measuring a water phantom but not by measuring metabolite signal *in vivo* [96].

We have developed a DW-LSEPSI technique for the accurate imaging of metabolite diffusion *in vivo* [21]. Because there is no phase-encoding, there is no ghosting artifact. The combination of line-scan and echo-planar techniques can specify the location of all pixels on the line for each acquisition to enable correction of phase errors at each spatial pixel in signal averaging. We applied DW-LSEPSI to a moving phantom and to a rat brain *in vivo* to acquire diffusion-weighted images and apparent diffusion coefficient (ADC) maps of metabolites. Preliminary reports of this work have been presented [97, 98].

4.2 MATERIALS AND METHODS

4.2.1 DIFFUSION-WEIGHTED LINE-SCAN ECHO-PLANAR SPECTROSCOPIC IMAGING

The DW-LSEPSI method we developed uses line-scan and echo-planar techniques to acquire spatial and spectral information and diffusion gradients to add diffusion information (Fig. 4.1). The region excited by the π/2- and π-pulses, having a diamond-shaped cross-section, is shifted diagonally, i.e., along the x-direction, shot-by-shot in a short time, which maximizes the SNR per measurement time up to half the SNR using normal slice selection [99]. The reason is that this line-scan technique excites up to half the volume of the slice excited by the normal slice selection in repetition time (*TR*) like multislice technique. The oscillating readout gradient is used to acquire data along the sinusoidal trajectory in the ky-time space [20]. The acquired data is reordered in the ky-time space and is inverse Fourier transformed to obtain both the spatial information in the y-direction and chemical shift information simultaneously. Precise reconstruction algorithm was described in the section 2.2.4 Experiments: Cerebral Ischemia Model Rats. Thus, the spatial locations of acquired pixels can be specified for each shot. A single Gaussian radiofrequency (RF) pulse is used for water suppression to reduce the duration of the line-scan shot. Although conventional spectroscopy/spectroscopic imaging uses multiple Gaussian RF pulses to suppress the water signal efficiently at a wide range of T_1 and flip angle of transmitted RF pulses, a single Gaussian RF pulse is efficient for LSEPSI because the short repetition time of the water suppression pulses (*TRw*) makes a series of single pulses comparable to multiple pulses. Figure 4.2 compares suppression rates at $TRw = \infty$ and $TRw = 250$ ms. Shorter

repetition time improves the suppression rate at a wide range of T_1 and flip angle [98]. The amplitude of the RF pulse for water suppression is adjusted to retain the water signal for phase correction depending on the duration of the line-scan shot and diffusion weighting. Signal averaging is performed along with phase correction, and the amount of phase correction is calculated to equalize the phase of the residual water signal at each pixel. This mitigates the signal loss induced by phase errors caused by motion.

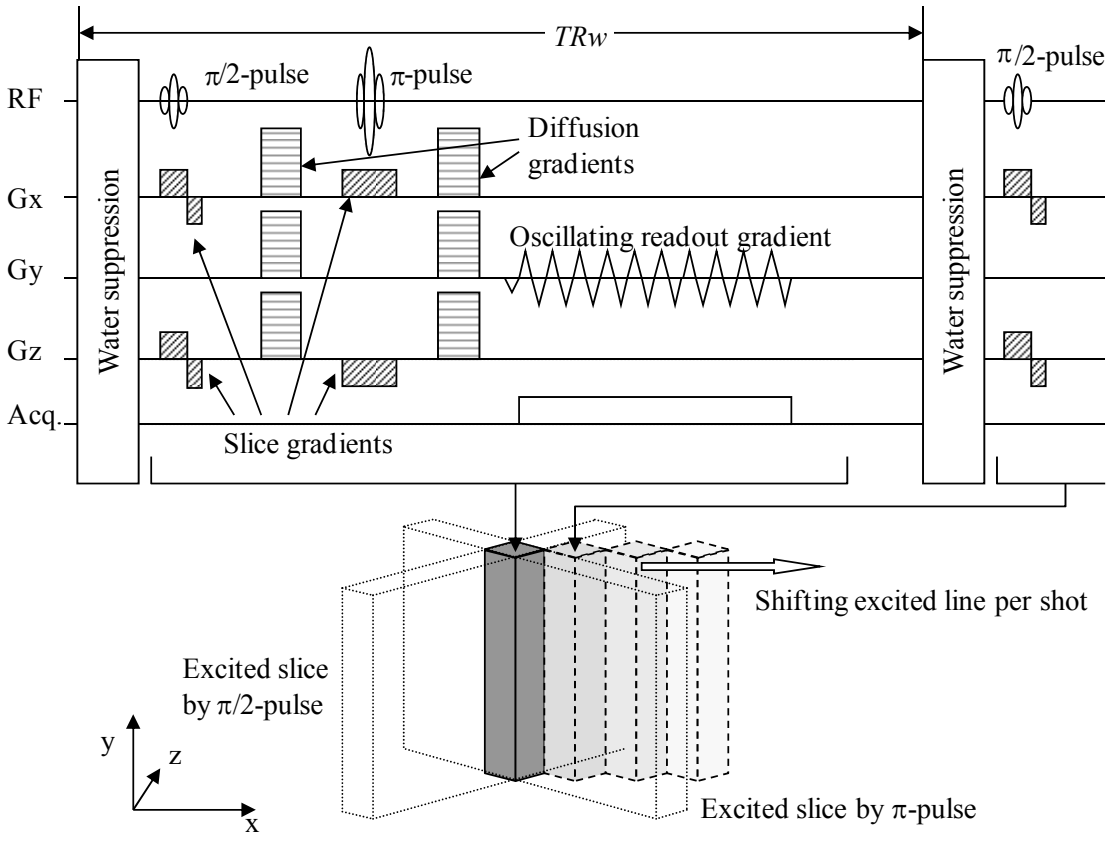

Figure 4.1. A schematic diagram of sequence and an excited line of the developed DW-LSEPSI. The excited line by π/2-pulse and π-pulse is shifted shot-by-shot at repetition time of *TRw* to acquire the x-direction spatial information. An oscillating readout gradient is used to acquire the y-direction spatial information and chemical shift information simultaneously.

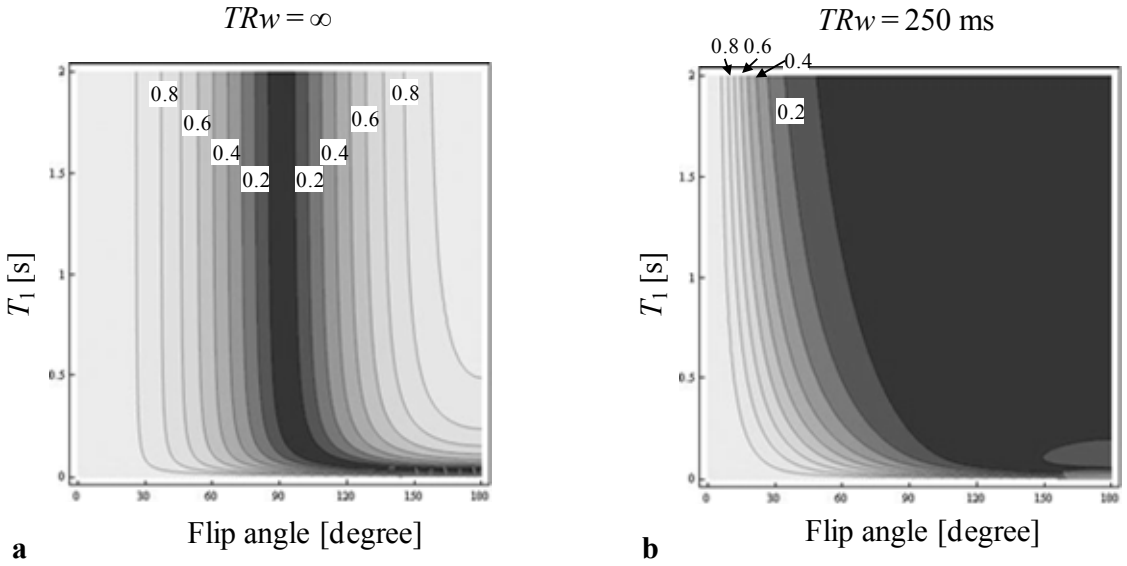

Figure 4.2. Contour maps of water suppression rate relative to T_1 and flip angle for the cases of **a**: $TRw = \infty$ and **b**: TRw = 250 ms, where TRw is repetition time of line-scan shot. Suppression rate in **b** is significantly different from that in **a**.

4.2.2 EXPERIMENTS: MOVING PHANTOM AND RAT BRAIN IN VIVO

We used a 7-T MR imaging unit for small animal study (Agilent Technologies, Inc., USA) equipped with actively shielded gradient coils of 120-mm inner diameter capable of producing a maximum amplitude of 400 mT/m within 150 μs, linear birdcage coil of 70-mm diameter for RF transmission/receive and 2-channel surface coil tuned to rat brains for RF receive (Rapid Biomedical, Inc., Germany).

To demonstrate the effectiveness of DW-LSEPSI in reducing motion artifacts, we used a moving phantom and a rat brain *in vivo*. The phantom was a glass bottle of 20-mm inner diameter filled with 100-mM of N-acetylaspartate (NAA) solution at 24°C. The phantom was oscillated at 110 cycles/minute for a length of 0.3 mm along the z-direction driven by tensing a rubber band and inflating a small balloon using a respirator (Fig. 4.3). The phantom was moved right by inflating the small balloon, and was moved back to left by rubber band when deflating the small balloon. We chose the cycle in a higher range of normal respiratory rate not to synchronize with the used *TR* of 4000 ms described later to enlarge the signal loss by motion. We chose the length to represent visualization of the motion of the loosely fixed rat head. In this phantom experiment, the birdcage coil was used both for RF transmit and receive.

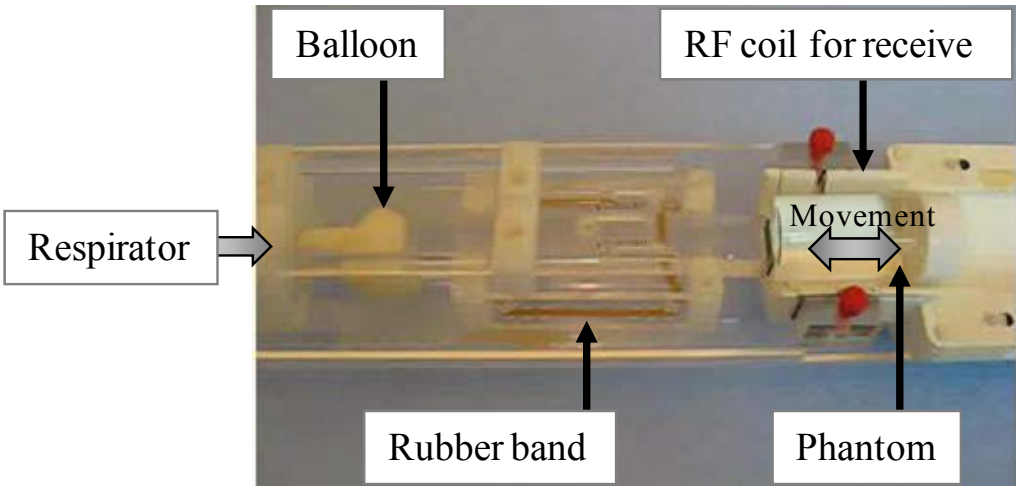

Figure 4.3. A photo of moving phantom driven by a respirator. A small balloon was inflated by a respirator to move the phantom to the right, and a rubber band returned the phantom when the balloon was deflated.

We employed a male 280-g Wistar rat for *in vivo* study, fixing the rat's head at 3 points (foreteeth and both earholes) in a dorsal state using a plastic bar attached on the surface coil. The rectal temperature was maintained between 37.5 and 38.5°C using a warm-water blanket. A mixture of isoflurane and room air was sent by a respirator to the rat head for anesthesia. Remarkably, this experiment was done under free breathing conditions with no tracheal intubation and no gating which easily causes large motion artifacts in conventional DWSI. This rat experiment utilized the birdcage coil for RF transmit and the surface coil for RF receive.

We compared DW-LSEPSI with DW-EPSI [20], which uses phase-encoding instead of line-scanning in the x-direction. The measurement parameters for both techniques were: *TR*, 4000 ms; echo time (*TE*), 136 ms; spectral bandwidth, 7.24 ppm (128 points); field of vision (FOV) in y, 40 mm (16 pixels); and slice thickness, 2.5 mm. FOV in x was 40 mm (16 encodes) for DW-EPSI and 30 mm (12 lines) for DW-LSEPSI, which equalized their spatial resolutions at 2.5 mm. To equalize the measurement times of both techniques, we utilized numbers of averaging for the phantom experiment were 1 for DW-EPSI and 16 for DW-LSEPSI, and those for the rat brain experiment were 8 for DW-EPSI and 128 for DW-LSEPSI. Diffusion gradients were added in the z-direction, of which duration and interval δ/Δ = 6/62 ms. We used *b*-values of 0, 550, 1090, and 1700 × 10^6 s/m^2 for the phantom experiment and 0, 550, 1700, and 3030 × 10^6 s/m^2 for the rat brain experiment. The total measurement times of both techniques were the same, about 4 minutes for the phantom experiment and 34 minutes for the brain experiment. DWIs of water and NAA were calculated by cut and sum of the signals along corresponding chemical shift regions for all measurements. We calculated ADC maps of water and NAA

by fitting the DWIs to a single exponential decay along the *b*-value only for DW-LSEPSI because DWIs showed large motion artifacts in DW-EPSI.

4.3 RESULTS

Figure 4.4 shows spectroscopic images of the phantom obtained by both DW-EPSI and DW-LSEPSI. In each spectroscopic image, the graph represents the spectra integrated in the whole spatial region. The x-axis is the chemical shift ranging from 6.24 to -1.00 ppm for every graph, and the y-axis is signal intensity normalized by peak water signal for the graphs of non-water suppression, and the y-axis is normalized by a certain value for the graphs of water suppression for easy visualization of the signal decay of NAA with the *b*-value. The image was calculated by integrating the signal in the selected region of chemical shift shown as a dashed line in the graph. As shown in Figure 4.4, good spectroscopic images of the phantom were obtained by both DW-EPSI and DW-LSEPSI at $b = 0$. Ghosting artifact and signal loss are evident in DW-EPSI when *b* is larger than 0, but no such artifacts can be seen in DW-LSEPSI.

Figure 4.5 shows spectroscopic images of the rat brain *in vivo*. In each spectroscopic image, the graph represents the spectra obtained from the selected brain region shown as a red rectangle, and the image was calculated by integrating the signal in the selected chemical shift region shown as a dashed line. The yellow lines represent the calculated outline of the rat head using T_1-weighted image. Similarly for the phantom result, motion artifacts can be seen in DW-EPSI but not in DW-LSEPSI when *b* is larger than 0. ADC maps of NAA were calculated for both the phantom and rat brain using

DW-LSEPSI but not using DW-EPSI because of the severe motion artifacts (Fig. 4.6). They show successfully calculated ADC maps, but the maps show slight spatial variance. This variance may result from the diffusion property of NAA and/or measurement error by using DW-LSEPSI. Addition of the diffusion gradient in only the z-direction may cause the ADC of NAA to become smaller in the radial axon near the cortex than in other regions, and insufficient phase correction near the base at larger *b*-values as a result of the smaller SNR near the base using the surface coil may cause the ADC of NAA to become larger near the base than in other regions. Motion may also be larger near the base from free breathing than that near the cortex because the rat head was fixed on the surface coil in the dorsal state.

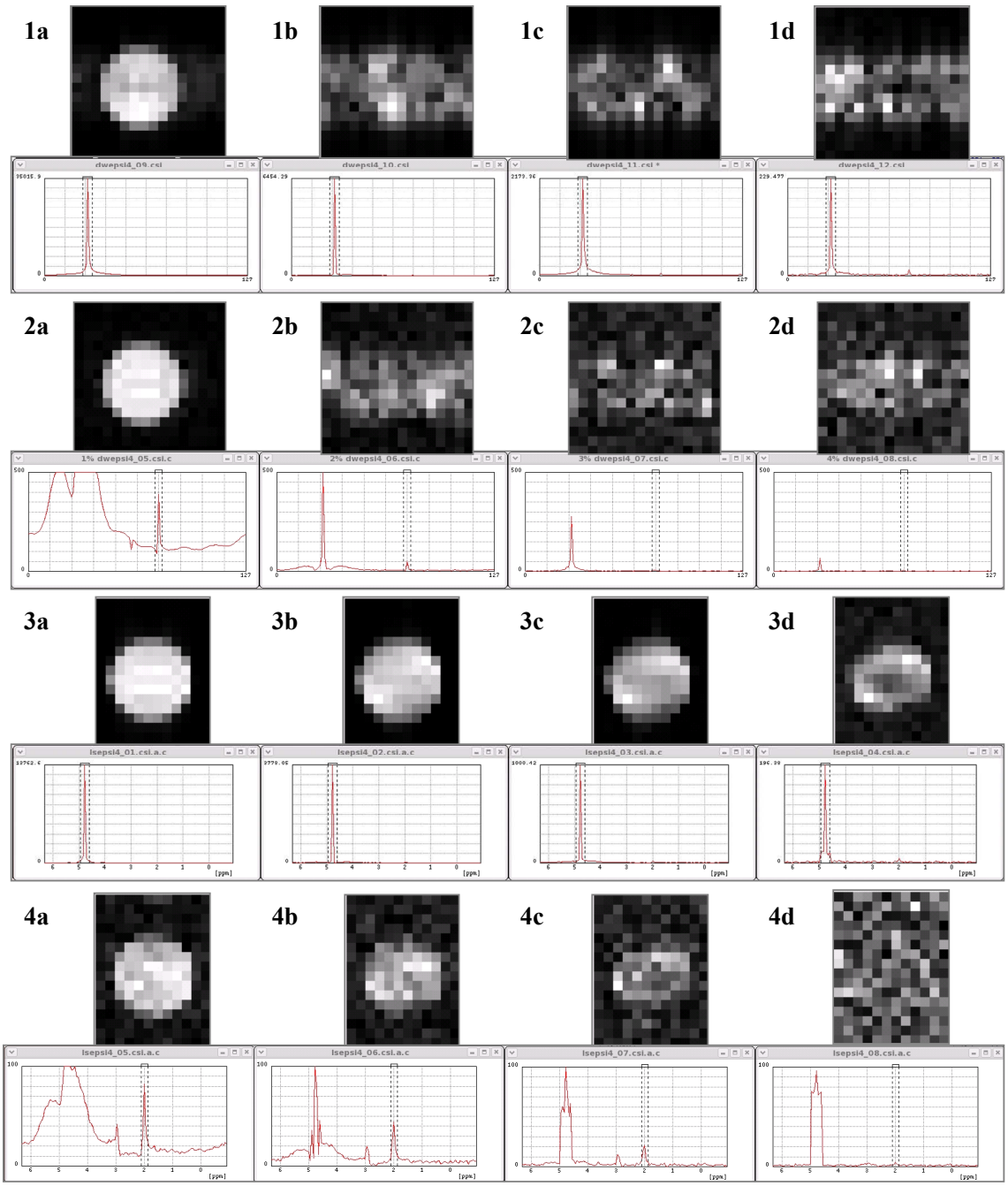

Figure 4.4. Diffusion-weighted spectroscopic images of a moving phantom: **1**: water images by using DW-EPSI without water suppression, **2**: NAA images by using DW-EPSI with water suppression, **3**: water images by using DW-LSEPSI without water suppression, and **4**: NAA images by using DW-LSEPSI with water suppression. In each image, *b*-values are **a**: 0, **b**: 550, **c**: 1090, and **d**: 1700 ($\times 10^6$ s/m^2).

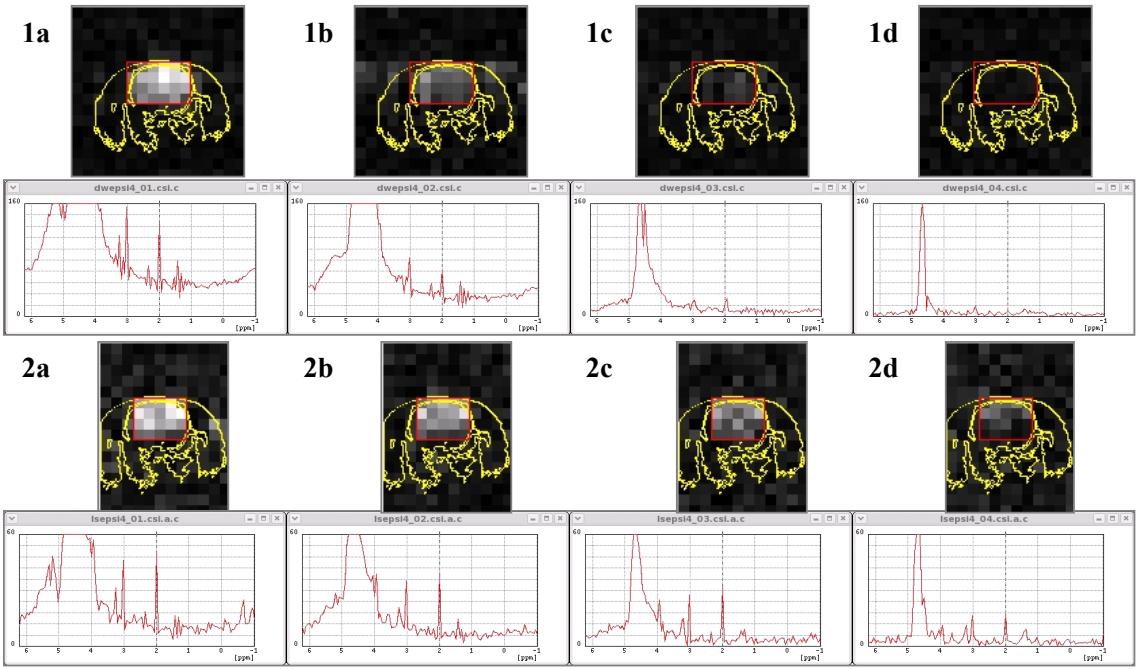

Figure 4.5. Diffusion-weighted spectroscopic images of a rat brain: **1**: NAA images by using DW-EPSI with water suppression, and **2**: NAA images by using DW-LSEPSI with water suppression. In each image, *b*-values are **a**: 0, **b**: 550, **c**: 1700, and **d**: 3030 ($\times 10^6$ s/m^2).

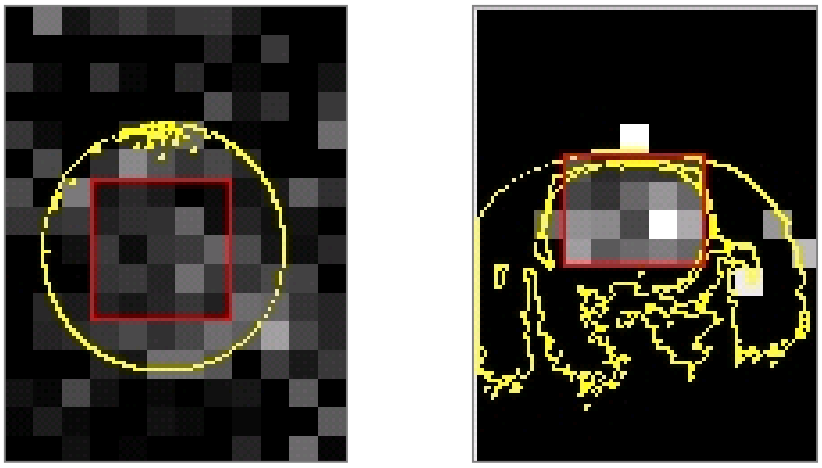

a **b**

Figure 4.6. Calculated ADC maps of NAA in **a**: a moving phantom and **b**: a rat brain *in vivo* by using DW-LSEPSI. The red rectangles represent the regions where average and standard deviation were calculated. The yellow lines represent outline of the phantom and the rat head, respectively.

Table 4.1. Calculated ADC of NAA and water in a phantom and a rat brain by using DW-LSEPSI.

	ADC (mean ± standard deviation) (10^{-9} m^2/s)	
	NAA	Water
Phantom (24˚C)	0.72 ± 0.04	2.35 ± 0.15
Rat brain	0.34 ± 0.04	–

As shown in Table 4.1, the calculated ADCs in the moving phantom at 24°C using DW-LSEPSI were 2.35 ± 0.15 × 10^{-9} m^2/s for water and 0.72 ± 0.04 × 10^{-9} m^2/s for NAA, which agree well with previously reported values obtained at 20°C using DWS −2.00 ± 0.05 ×10^{-9} m^2/s (water) and 0.85 ± 0.05 ×10^{-9} m^2/s (NAA)(2) and 2.15 ± 0.04 ×10^{-9} m^2/s (water) and 0.61 ± 0.06 ×10^{-9} m^2/s (NAA)(6). The higher ADC of water in our results is attributable mainly to the temperature dependence of the ADC, which is estimated to be about 0.23 × 10^{-9} m^2/s between 24 and 20°C [100]. This result demonstrates the improved accuracy in ADC measurement by the reduction of motion artifacts using

DW-LSEPSI. The calculated ADC of NAA in the rat brain *in vivo* using DW-LSEPSI was $0.34 \pm 0.04 \times 10^{-9}$ m^2/s, which seems higher than reported values $0.27 \pm 0.04 \times 10^{-9}$ m^2/s [72] and $0.17 \pm 0.04 \times 10^{-9}$ m^2/s [85]. This may be explained by insufficient reduction of motion artifact at higher *b*-values using DW-LSEPSI, acquisition of regions by DWSI that are not acquired by DWS, and/or diffusion properties of NAA. The interesting diffusion properties of NAA are non-monoexponential decay along with *b*-values and dependency with diffusion time [89-91] and higher diffusion anisotropy [92-94]. These diffusion properties of metabolites should be investigated further.

4.4 DISCUSSION

4.4.1 TECHNOLOGY IMPROVEMENTS

Other methods proposed to reduce motion artifacts are diffusion-weighted echo-planar spectroscopic imaging with a pair of bipolar diffusion gradients (DW-EPSI with BPGs) [101] and diffusion-sensitive single-shot proton-echo-planar-spectroscopic imaging (DW-SS-PEPSI) [102]. DW-EPSI with BPGs uses a pair of bipolar diffusion gradients to reduce the phase error caused by uniform motion. DW-LSEPSI has an advantage over DW-EPSI with BPGs in non-uniform motion but a disadvantage in non-rigid motion, such as inflating motion. It may be better to select DW-LSEPSI or DW-EPSI with BPGs in accordance with the target motion. DW-SS-PEPSI uses two-dimensional echo-planar and parallel imaging to acquire whole data in a single-shot. DW-SS-PEPSI may better reduce motion artifacts, but quality of acquired data is limited, perhaps as a result of the high frequency oscillating gradient and reduced SNR in parallel

imaging. Another technique using two-dimensional echo-planar imaging with time-domain-interleaved technique, instead with parallel imaging technique, was proposed [103]. Although this technique has an advantage in spatial information in a single-shot, this technique may have a disadvantage in spectral quality because several shot is needed to obtain spectral information. The simple synchronizing technique to respiration or pulsation and the phase correction technique using navigator-echo may have effectiveness on reducing motion artifacts to some extent.

DW-LSEPSI also has a disadvantage in SNR per measurement time because the excited line has a diamond-shaped cross-section, and the excited volume is up to half of the normal slice selection. The calculated SNR of DW-LSEPSI was 30% of that of DW-EPSI for the moving phantom at $b = 0$. Although this SNR reduction is mostly a tradeoff for improved spatial resolution in both the x- and z-directions, loss at the edge of slicing becomes larger when the spatial resolution becomes smaller. Improved SNR requires an excitation pulse with better slice profile. SNR may also be improved using a parallel line scan, which uses parallel excitation of multiple lines simultaneously and parallel imaging to identify excited each line [104, 105]. Using this technique, SNR can be increased along with the ratio of the number of excited lines to a geometric factor.

4.4.2 APPLICATION EXPANSION

This chapter describes application of DW-LSEPSI technique to investigate metabolites diffusion in normal brain *in vivo*. However, this technique will be applied to investigate metabolites diffusion in disease, such as stroke, cancer, and neurologic disorders. These applications will provide useful information about development of disease because local transport of metabolites is an important biomarker, such as

reduction of axonal transport in Alzheimer's disease [15, 16]. As discussed in the previous section 4.4.1 Technology Improvements, appropriate DWSI technique should be selected according to the target. The DWSI, including the presented DW-LSEPSI, will become a powerful tool both for medical science to investigate microscopic transport in diseases and for clinical diagnosis to detect early changes of dynamic metabolism in diseases.

4.5 CONCLUSION

We developed a DW-LSEPSI technique that combines line-scan and echo-planar techniques to obtain accurate diffusion-weighted images and ADC maps of metabolites by reducing motion artifacts, and we compared it with conventional DW-EPSI in experiments with a moving phantom and a rat brain *in vivo*. Our results demonstrate that the developed DW-LSEPSI efficiently reduces motion artifacts. DW-LSEPSI will be a powerful tool for studies of diffusion images of metabolites in both basic science and clinical use.

CHAPTER 5 CONCLUSIONS

5.1 SUMMARY

The aim of this thesis was to develop magnetic resonance spectroscopic imaging (MRSI) technique to measure dynamic metabolism, especially for lactate distribution and for molecular diffusion maps of metabolites. The fast and accurate MRSI technique was developed for each aims based on echo-planar spectroscopic imaging (EPSI) technique which enables acquiring spectral and spatial information simultaneously.

For lactate distribution, fast lactate-discriminating EPSI technique was developed using the EPSI technique and echo-shit technique which enables discriminating lactate signal from overlapped lipid signal. The optimum echo time for the echo-shift technique was estimated to sufficiently suppress lipid signal while maintaining lactate signal. Acquisition of discriminated lactate distribution was demonstrated by applying this technique to a rat stroke model. This technique is expected to be used in accumulating knowledge about stroke and in clinical diagnosis of acute stroke.

For molecular diffusion maps of metabolites, fast diffusion-weighted echo-planar spectroscopic imaging (DW-EPSI) technique was developed by adding diffusion gradients to the EPSI technique. Reduction of measurement time was demonstrated by applying this technique to a phantom consisting of two materials. Furthermore, diffusion-weighted line-scan echo-planar spectroscopic imaging (DW-LSEPSI) technique was developed to reduce motion artifacts. The combination of line-scan and EPSI techniques enables accurate phase correction at each spatial point at each shot, and thus, decreasing phase errors induced by motion. Reduction of motion artifacts in

diffusion-weighted spectroscopic images is demonstrated by applying this technique to a normal rat brain *in vivo*. The developed technique is expected to be used in both basic science investigating intracellular environment and clinical use diagnosing early stages of diseases.

5.2 FUTURE DIRECTION

The developed spectroscopic imaging techniques for dynamic metabolism have several future directions in technical development as well as their research and clinical application. Rapidly developing useful techniques in MRI can be adapted to improve the developed spectroscopic imaging techniques.

Fundamental specification about measurement time and SNR of developed spectroscopic imaging technique will be improved furthermore by applying fast imaging techniques, such as parallel imaging and compressed sensing, developed for basic MRI. These techniques will reduce the measurement time, increase the spatial information and/or two-dimensional spectral information. Especially, reduction of measurement time is very important in clinical application. The reduced measurement time prevents progression of diseases and enables timely treatment for acute diseases. It also prevents condition worsening for chronic diseases. Typical target measurement time of each measurement is less than about five minutes under current clinical situation, because the other measurements are necessary to obtain various information for accurate diagnosis.

The lactate-discriminating EPSI technique will be applied more diseases other than stroke. For example, application to cancer will enable detection of hypoxic region which is important to estimate resistance to radiation therapy. The combination with DWSI technique may provide improved accuracy in detecting the hypoxic region. The lactate molecule diffuses so highly that the accurate detection of the hypoxic region where lactate produces is not easy. Combination with DWSI technique will suppress the highly diffusing lactate molecule that mostly exists in extracellular space.

The DWSI technique will be improved to acquire more detailed diffusion properties of metabolites by introducing cutting-edge diffusion measurement technique developed for measuring water diffusion such as non-Gaussian diffusion measurement technique. Precise analysis between these diffusion properties of metabolites and water will provide rich information about microscopic environment, such as structure or transport function of intracellular space while separating neurons and glial cells. This thesis focused on the research using endogenous molecules; however, the developed DWSI technique is not limited to be used only for endogenous molecules. Application to exogenous molecule will enable acquiring microscopic transport of exogenous molecule, such as ^{19}F-labeled 5-Fluorouracil, ^{17}O-labeled water and ^{13}C-labeled compounds.

Although a few application of DWSI technique has been proposed currently, it is just the beginning of investigating disease in intracellular dynamic metabolism. The DWSI technique will be a powerful tool to accumulate knowledge about intracellular dynamic metabolism in diseases and to realize early diagnosis by detecting subtle changes in intracellular dynamic metabolism. Neurologic diseases may be one of the

target diseases, because DWSI enables separate observation of intracellular environments of neuron and glial cell by using metabolites as cell-specific probes.

CHAPTER 6 REFERENCES

1. Zhu H, Barker PB. MR spectroscopy and spectroscopic imaging of the brain. Methods Mol Biol 2011;711:203-226.
2. Bottomley PA, Edelstein WA, Foster TH, Adams WA. *In vivo* solvent-suppressed localized hydrogen nuclear magnetic resonance spectroscopy: A window to metabolism? Proc Natl Acad Sci 1985;82:2148–2152.
3. Knight RA, Ordidge RJ, Helpern JA, Chopp M, Rodolosi LC, Peck D. Temporal evolution of ischemic damage in rat brain measured by proton nuclear magnetic resonance imaging. Stroke 1991;22:802-808.
4. Prichard J, Rothman D, Novotny E, Petroff O, Kuwabara T, Avison M, Howseman A, Hanstock C, Shulman R. Lactate rise detected by ^{1}H NMR in human visual cortex during physiologic stimulation. Pro Natl Acad Sci 1991;88:5829-5831.
5. Moonen CT, van Zijl PC, Le Bihan D, DesPres D. *In vivo* NMR diffusion spectroscopy: ^{31}P application to phosphorus metabolites in muscle. Magn Reson Med 1990;13:467-477.
6. Zhou JY, Payen JF, Wilson DA, Traystman RJ, van Zijl PCM. Using the amide proton signals of intracellular proteins and peptides to detect pH effects in MRI. Nat Med 2003;9:1085–1090.
7. Szimtenings M, Olt S, Haase A. Flow encoded NMR spectroscopy for quantification of metabolite flow in intact plants. J Magn Reson 2003;161:70-6.
8. Stevens AN, Morris PG, Iles RA, Sheldon PW, Griffiths JR. 5-fluorouracil metabolism monitored *in vivo* by 19F NMR. Br J Cancer 1984;50:113–117.

9. Otake Y, Soutome Y, Hirata K, Ochi H, Bito Y. Double-tuned RF coil design for ^{19}F and ^{1}H imaging. Magn Reson Med Sci 2014;13:199-205.

10. Rothman DL, Behar KL, Hetherington HP, Den Hollander JA, Bendall MR, Petroff OAC, Shulman RG. ^{1}H-observe/^{13}C-decouple spectroscopic measurements of lactate and glutamate in the rat brain *in vivo*. Proc Natl Acad Sci 1985;82:1633-1637.

11. Kohler SJ, Yen Y, Wolber J, Chen AP, Albers MJ, Bok R, Zhang V, Tropp J, Nelson S, Vigneron DB, Kurhanewicz J, Hurd RE. *In vivo* ^{13}C metabolic imaging at 3T with hyperpolarized ^{13}C-1-pyruvate. Magn Reson Med 2007;58:65–9.

12. Zhu XH, Zhang N, Zhang Y, Zhang X, Ugurbil K, Chen W. *In vivo* ^{17}O NMR approaches for brain study at high field. NMR Biomed 2005;18:83-103.

13. Albert MS, Cates GD, Driehuys B, Happer W, Saam B, Springer, Jr. CS, Wishnia A. Biological magnetic resonance imaging using laser-polarized ^{129}Xe. Nature 1994;370:199–201.

14. Neumann-Haefelin T, Wittsack HJ, Wenserski F, Siebler M, Seitz RJ, Moddr U, Freund HJ. Diffusion- and perfusion-weighted MRI: the DWI/PWI mismatch region in acute stroke. Stroke 1999;30:1591-1597.

15. Stokin GB, Goldstein SB. Axonal transport and Alzheimer's disease. Annu Rev Biochem 2006;75:607-627.

16. Minoshima S, Cross D. *In vivo* imaging of axonal transport using MRI: aging and Alzheimer's disease. Eur J Nucl Med Mol Imaging 2008;35:S80-92.

17. Matsui S, Sekihara K, Kohno H. High-speed spatially resolved high resolution NMR spectroscopy. J Am Chem Soc 1985;107:2817-2818.

18. Matsui S, Sekihara K, Kohno H. Spatially resolved NMR spectroscopy using

phase-modulated spin-echo trains. J Magn Reson 1986;67:476-490.

19. Bito Y, Ebisu T, Hirata S, Takegami T, Yamamoto Y, Tanaka C, Naruse S. Lactate discrimination incorporated into echo-planar spectroscopic imaging. Magn Reson Med. 2001;45:568-574.
20. Bito Y, Hirata S, Nabeshima T, Yamamoto E. Echo-planar diffusion spectroscopic imaging. Magn Reson Med. 1995;33:69-73.
21. Bito Y, Hirata K, Ebisu T, Kawai Y, Otake Y, Hirata S, Shirai T, Soutome Y, Ochi H, Yamamoto E, Umeda M, Higuchi T, Tanaka C. Diffusion-weigted line-scan echo-planar spectroscopic imaging technique to reduce motion artifacts in metabolited diffusion imaging. Magn Reson Med Sci 2015;14:43-50.
22. Frahm J, Bruhn H, Gyngell M, Merboldt KD, Hänicke W, Sauter R. Localized proton NMR spectroscopy in different regions of the human brain *in vivo*: relaxation times and concentrations of cerebral metabolites. Magn Reson Med 1989;11:47-63.
23. Spielman DM, Pauly J, Macovski A, Glover G, Enzmann D. Lipid-suppressed single- and multisection proton spectroscopic imaging of the human brain. J Magn Reson Imaging 1992;2:253-262.
24. Adalsteinsson E, Spielman DM, Wright GA, Pauly JM, Meyer CH, Macovski A. Incorporating lactate/lipid discrimination into a spectroscopic imaging sequence. Magn Reson Med 1993;30:124-130.
25. Bourgeois D, Kozlowski P. A highly sensitive lactate editing technique for surface coil spectroscopic imaging *in vivo*. Magn Reson Med 1993;29:402-406.
26. Reese T, Norris DG, Leibfritz D. A fast method for *in vivo* lactate imaging. NMR in Biomed. 1995;8:225-231.

27. Duyn JH, Frank JA, Moonen CTW. Incorporation of lactate measurement in multi-spin-echo proton spectroscopic imaging. Magn Reson Med 1995;33:101-107.

28. Hurd RE, Freeman DM. Metabolite specific proton magnetic resonance imaging. Proc Natl Acad Sci USA 1989;86:4402-4406.

29. de Graaf AA, Luyten PR, den Hollander JA, Heindel W, Bovée WMMJ. Lactate imaging of the human brain at 1.5 T using double quantum filter. Magn Reson Med 1993;30:231-235.

30. Wild JM, Marshall I. *In vivo* lactate editing in single voxel proton spectroscopy and proton spectroscopic imaging by homonuclear polarization transfer. Magn Reson Imag 1999;17:131-139.

31. Rothman DL, Behar KL, Hetherington KL, Shulman RG. Homonuclear ^{1}H double resonance difference spectroscopy of the rat brain *in vivo*. Proc Natl Acad Sci USA 1984;81:6330-6334.

32. Hetherington HP, Avison MJ, Shulman RG. ^{1}H homonuclear editing of rat brain using semi-selective pulses. Proc Natl Acad Sci USA 1985;82:3115-3119.

33. Williams SR, Gadian DG, Proctor E. A method of lactate detection *in vivo* by spectral editing without the need for double irradiation. J Magn Reson 1986;66:562-567.

34. Star-Lack J, Spielman D, Adalsteinsson E, Kurhanewicz J, Terris DJ, Vigneron DB. *In vivo* lactate editing with simultaneous detection of choline, creatine, NAA, and lipid singlets at 1.5 T using PRESS excitation with applications of the study of brain and head and neck tumors. J Magn Reson 1998;133:243-254.

35. Sotak CH, Freeman DM, Hurd RE. The unequivocal determination of *in vivo*

lactic acid using two-dimensional double-quantum coherence-transfer spectroscopy. J Magn Reson 1988;78:355-361.

36. von Kienlin M, Albrand JP, Authier B, Blondet P, Lotito S, Decorps M. Spectral editing *in vivo* by homonuclear polarization transfer. J Magn Reson 1987;75:371-377.

37. Bunse M, Jung WI, Schick F, Dietze GJ, Lutz O. HOPE, a new lactate editing method. J Magn Reson B 1995;109:270-274.

38. Brereton IM, Rose SE, Galloway GJ, Maxton LN, Doddrell DM. *In vivo* selective metabolite editing via correlated z-order. Magn Reson Med 1990;16:460-469.

39. Posse S, Tedeschi G, Risinger R, Ogg R, Le Bihan D. High speed ^{1}H spectroscopic imaging in human brain by echo planar spatial-spectral encoding. Magn Reson Med 1995;33:34-40.

40. Bito Y, Hirata S, Yamamoto E. Four-dimensional echo-planar diffusion spectroscopic imaging. In: Proceedings of the ISMRM 3rd Annual Meeting, Nice, 1995. p 910.

41. Tropper MM. Image reconstruction for the NMR echo-planar technique, and for a proposed adaptation to allow continuous data acquisition. J Magn Reson 1981;42:193-202.

42. Haase A, Frahm J, Hänicke W, Matthei D. ^{1}H NMR chemical shift selective imaging. Phys Med Biol 1985;30:341-344.

43. Duyn J, Gillen J, Sobering G, van Zijl P, Moonen C. Multislice proton spectroscopic imaging of the human brain. Radiology 1993;188:277-282.

44. Turner R, Le Bihan D. Single-shot diffusion imaging at 2.0 Tesla. J Magn Reson 1990;86:445-452.

45. Turner R, Le Bihan D, Maier J, Vavrek R, Kyle L, Pekar J. Echo-planar imaging of intravoxel incoherent motion. Radiology 1990;177:407-414.

46. Basser PJ, Mattiello J, Le Bihan D. MR diffusion tensor spectroscopy and imaging. Biophys J 1994;66:259-267.

47. van Gelderen P, de Vleeschouwer MH, DesPres D, Pekar J, van Zijl PCM, Moonen CTW. Water diffusion and acute stroke. Magn Reson Med 1994;31:154-163.

48. Moseley ME, Cohen Y, Mintorovitch J, Chileuitt L, Shimizu H, Kucharczyk J, Wendland MF, Weinstein PR. Early detection of regional cerebral ischemia in cats: comparison of diffusion- and T_2-weighted MRI and spectroscopy. Magn Reson Med 1990;14:330-346.

49. Decanniere C, Eleff S, Davis DR, van Zijl PCM. Correlation of rapid changes in the average water diffusion constant and the concentrations of lactate and ATP breakdown products during global ischemia in cat brain. Magn Reson Med 1995;34:343-352.

50. Ebisu T, Rooney WD, Graham SH, Mancuso A, Weiner MW, Maudsley AA. MR spectroscopic imaging and diffusion-weighted MRI for early detection of kainate-induced status epilepticus in the rat. Magn Reson Med 1996;36:821-828.

51. Dreher W, Kühn B, Gyngell ML, Busch E, Niendorf T, Hossmann KA, Leibfritz D. Temporal and regional changes during focal ischemia in rat brain studied by proton spectroscopic imaging and quantitative diffusion NMR imaging. Magn Reson Med 1998;39:878-888.

52. van der Toorn A, Syková E, Dijkhuizen RM, Vořišek I, Vargová L, Škobisová E, van Lookeren Campagne M, Reese T, Nicolay K. Dynamic Changes in water

ADC, energy metabolism, extracellular space volume, and tortuosity in neonatal rat brain during global ischemia. Magn Reson Med 1996;36:52-60.

53. Bito Y, Hirata K, Shirai T, Yamamoto Y, Soutome Y, Ebisu T, Umeda M, Kawai Y, Higuchi T, Tanaka C. Lactate-discriminating echo-planar spectroscopic imaging. In: Proceedings of the 16th Annual Meeting of the International Society for Magnetic Resonance Imaging, Toronto, Canada, 2008. p 596.
54. Mansfield P. Spatial mapping of the chemical shift in NMR. Magn Reson Med 1984;1:370-386.
55. Duyn JH, Moonen CTW. Fast proton spectroscopic imaging of human brain using multiple spin-echoes. Magn Reson Med 1993;30:409-414.
56. Adalsteinsson E, Irarrazabal P, Topp S, Meyer C, Macovski A, Spielman DM. Volumetric spectroscopic imaging with spiral-based k-space trajectories. Magn Reson Med 1998;39:888-898.
57. Speck O, Scheffler K, Hennig J. Fast ^{31}P chemical shift imaging using SSFP methods. Magn Reson Med 2002;48:633-639.
58. Dydak U, Weiger M, Pruessmann KP, Meier D, Boesiger P. Sensitivity-encoded spectroscopic imaging. Magn Reson Med 2001;46:713-722.
59. Hu S, Lustig M, Chen AP, Crane J, Kerr A, Kelley DAC, Hurd RE, Kurhanewicz J, Nelson SJ, Pauly JM, Vigneron DB. Compressed sensing for resolution enhancement of hyperpolarized ^{13}C flyback 3D-MRSI. J Magn Reson 2008;192:258-264.
60. Bunse M, Jung WI, Dietze G, Lutz O. Determination of the chemical-shift difference between the lactate multiplets and its pH dependence. J Magn Reson B 1996;112:236-239.

61. Barker PT, Soher BJ, Blackband SJ, Chatham JC, Mathews VP, Bryan RN. Quantitation of proton NMR spectra of the human brain using tissue water as an internal concentration reference. NMR Biomed 1994;6:89–94.

62. Takegami T, Ebisu T, Bito Y, Hirata S, Yamamoto Y, Tanaka C, Naruse S, Mineura K. Mismatch between lactate and the apparent diffusion coefficient of water in progressive focal ischemia. NMR Biomed. 2001;14:5-11.

63. Röther J, de Crespigny AJ, D'Arceuil H, Moseley ME. MR detection of cortical spreading depression immediately after focal ischemia in the rat. J Cereb Blood Flow Metab 1996;16:214-220.

64. Stejskal EO, Tanner JE. Spin diffusion measurements: spin echoes in the presence of a time-dependent field gradient. J Chem Phys 1965;42:288-292.

65. Cleveland GG, Chang DC, Hazelwood CF, Rorschach HE. Nuclear magnetic resonance measurement of skeletal muscle: anisotropy of the diffusion coefficient of the intracellular water. Biophys J 1976;16:1043-1053.

66. Tanner JE. Self diffusion of water in frog muscle. Biophys J 1979;28:107-116.

67. Le Bihan D, Breton E, Lallemand D, Grenier P, Cabanis E, Laval-Jeantet M. MR imaging of intravoxel incoherent motions: application to diffusion and perfusion in neurologic disorders. Radiology 1986;161:401-407.

68. Le Bihan D, Breton E, Lallemand D, Aubin ML, Vignaud J, Laval-Jeantet M. Separation of diffusion and perfusion in intravoxel incoherent motion MR imaging. Radiology 1988;168:497-505.

69. Dardzinski BJ, Sotak CH, Fisher M, Hasegawa Y, Li L, Minematsu K. Apparent diffusion coefficient mapping of experimental focal cerebral ischemia using diffusion-weighted echo-planar imaging. Magn Reson Med 1993;30:318-325.

70. Müler MF, Prasad PV, Siewert B, Raptopoulos V, Nissenbaum MA, Lewis WD, Edelman RR. Abdominal diffusion mapping using a whole body echo planar system. In Proceedings of 12th Annual Meeting of SMRM, New York, USA 1993, p 45.

71. Moonen CTW, van Gelderen P, van Zijl PCM, DesPres D, Olson A. The translational mobility of N-acetylaspartate in cat brain measured by localized proton NMR diffusion spectroscopy. In Proceedings of 10th Annual Meeting of SMRM, San Francisco, USA, 1991, p 141.

72. Merboldt KD, Hösterman D, Hänicke D, Bruhn H, Frahm J. Molecular self-diffusion of intracellular metabolites in rat brain *in vivo* investigated by localized proton NMR diffusion spectroscopy. Magn Reson Med 1993;29:125-129.

73. Posse S, Cuenod CA, Le Bihan D. Human brain: proton diffusion MR spectroscopy. Radiology 1993;188:719-725.

74. Xin M, Ng TC, Modic M. Reverse alternations of diffusion-weighted metabolites detected in human brain tumors and in the contralateral normals using proton chemical shift imaging. In Proceedings of 12th Annual Meeting of SMRM, New York, USA 1993; p 68.

75. Mansfield P. Multi-planar image formation using NMR spin echoes. J Phys 1997;C 10:L55-L58.

76. Bito Y, Hirata S, Yamamoto E. Diffusion spectroscopic imaging in inhomogeneous magnetic field. In Proceedings of 21st Annual Meeting of Japanese Society for Magnetic Resonance in Medicine, Tsukuba, Japan, 1993; p 147. [Japanese]

77. Neeman M, Freyer JP, Sillerud LO. Pulsed-gradient spin-echo diffusion studies in NMR imaging: effects of the imaging gradients on the determination of diffusion coefficients. J Magn Reson 1990;90:303-312.

78. Hong X, Dixon WT. Measuring diffusion in inhomogeneous systems in imaging mode using antisymmetric sensitizing gradients. J Magn Reson 1992;99:561-570.

79. Hirata S, Bito Y, Yamamoto E. Expansion of the spectral bandwidth by spatial and chemical shift selective saturation in high-speed magnetic resonance spectroscopic imaging. Magn Reson Med. 1996;35:611-616.

80. Bito Y, Kawai Y, Hirata K, Ebisu T, Shirai T, Hirata S, Soutome Y, Ochi H, Umeda M, Higuchi T, Tanaka C. Diffusion tensor spectroscopic imaging of rat brains. In: Proceedings of the 19th Annual Meeting of the International Society for Magnetic Resonance Imaging, Montreal, Canada, 2011. p 408.

81. Callaghan P. Principles of Nuclear Magnetic Resonance Microscopy. New York: Oxford University Press; 1993.

82. Bito Y, Hirata S, Yamamoto E. Optimum gradient factor for apparent diffusion coefficient measurements. In: Proceedings of the 3rd Annual Meeting of the Society for Magnetic Resonance in Medicine, Nice, France, 1995 In: Proceedings the 3rd Annual Meeting of the Society for Magnetic Resonance in Medicine, Nice, France, 1995. p 913.

83. Nicolay K, Braun KP, Graaf RA, Dijkhuizen RM, Kruiskamp MJ. Diffusion NMR spectroscopy. NMR Biomed 2001; 14:94-111.

84. Wick M, Nagatomo Y, Prielmeier F, Frahm J. Alteration of intracellular metabolite diffusion in rat brain *in vivo* during ischemia and reperfusion. Stroke 1995;26:1930-1933.

85. van der Toorn A, Dijkhuizen RM, Tulleken CA, Nicolay K. Diffusion of metabolites in normal and ischemic rat brain measured by localized ^{1}H MRS. Magn Reson Med 1996;36:914-922.

86. Abe O, Okubo T, Hayashi N, Saito N, Iriguchi N, Shirouzu I, Kojima Y, Masumoto T, Ohtomo K, Sasaki Y. Temporal changes of the apparent diffusion coefficients of water and metabolites in rats with hemispheric infarction: experimental study of transhemispheric diaschisis in the contralateral hemisphere at 7 Tesla. J Cereb Blood Flow Metab 2000;20:726-735.

87. Dreher W, Busch E, Leibfritz D. Changes in apparent diffusion coefficients of metabolites in rat brain after middle cerebral artery occlusion measured by proton magnetic resonance spectroscopy. Magn Reson Med 2001;45:383-389.

88. Harada M, Uno M, Hong F, Hisaoka S, Nishitani H, Matsuda T. Diffusion-weighted *in vivo* localized proton MR spectroscopy of human cerebral ischemia and tumor. NMR Biomed 2002;15:69-74.

89. Assaf Y, Cohen Y. *In vivo* and in vitro bi-exponential diffusion of N-acetyl aspartate (NAA) in rat brain: a potential structural probe? NMR Biomed 1998;11:67-74.

90. Assaf Y, Cohen Y. Non-mono-exponential attenuation of water and N-acetyl aspartate signals due to diffusion in brain tissue. J Magn Reson 1998;131:69-85.

91. Kroenke CD, Ackerman JJ, Yablonskiy DA. On the nature of the NAA diffusion attenuated MR signal in the central nervous system. Magn Reson Med 2004;52:1052-1059.

92. Ellegood J, Hanstock CC, Beaulieu C. Diffusion tensor spectroscopy (DTS) of human brain. Magn Reson Med 2006;55:1-8.

93. Ellegood J, McKay RT, Hanstock CC, Beaulieu C. Anisotropic diffusion of metabolites in peripheral nerve using diffusion weighted magnetic resonance spectroscopy at ultra-high field. J Magn Reson 2007;184:20-28.

94. Upadhyay J, Hallock K, Erb K, Kim DS, Ronen I. Diffusion properties of NAA in human corpus callosum as studied with diffusion tensor spectroscopy. Magn Reson Med 2007;58:1045-1053.

95. Posse S, Cuenod CA, Le Bihan D. Motion artifact compensation in ^{1}H spectroscopic imaging by signal tracking. J Magn Reson 1993; B102:222-227.

96. Bito Y, Hirata S, Tsukada K. Echo-planar diffusion spectroscopic imaging: reduction of motion artifacts using line-scan technique. In: Proceedings of the 6th Annual Meeting of ISMRM, Sydney, Australia 1998, p 1235.

97. Bito Y, Hirata K, Ebisu T, Kawai Y, Otake Y, Hirata S, Shirai T, Soutome Y, Ochi H, Umeda M, Higuchi T, Tanaka C. Diffusion-weighted line-scan echo-planar spectroscopic imaging for improved accuracy in metabolite diffusion imaging. In: Proceedings of the 17th Annual Meeting of ISMRM, Hawaii, USA 2009, p 334.

98. Bito Y, Hirata K, Ebisu T, Kawai Y, Otake Y, Hirata S, Shirai T, Soutome Y, Ochi H, Umeda M, Higuchi T, Tanaka C. Water suppression for diffusion-weighted line-scan echo-planar spectroscopic imaging. In: Proceedings of the 18th Annual Meeting of the International Society for Magnetic Resonance Imaging, Stockholm, Sweden, 2010. p 959.

99. Oshio K, Kyriakos W, Mulkern RV. Line scan echo planar spectroscopic imaging. Magn Reson Med 2000;44:521-524.

100. Tofts PS, Lloyd D, Clark CA, Barker GJ, Parker GJM, McConville P, Baldock C,

Pope JM. Test liquids for quantitative MRI measurements of self-diffusion coefficient *in vivo*. Magn Reson Med 2000;43:368-374.

101. Bito Y, Hirata K, Ebisu T, Kawai Y, Otake Y, Hirata S, Shirai T, Soutome Y, Ochi H, Umeda M, Higuchi T, Tanaka C. Motion artifact reduction using bipolar diffusion gradients in diffusion-weighted echo-planar spectroscopic imaging. In: Proceedings of the 18th Annual Meeting of the International Society for Magnetic Resonance Imaging, Stockholm, Sweden, 2010. p 24.
102. Posse S, Yoshimoto AE, Otazo R, van der Kouwe A, Lin FH, Wald LL. Diffusion-sensitive single-shot proton-echo-planar-spectroscopic-imaging (PEPSI) in human brain. In: Proceedings of the 17th Annual Meeting of ISMRM, Hawaii, USA 2009, p 3521.
103. Bito Y, Hirata K, Hirata S, Shirai T, Ebisu T, Kawai Y, Otake Y, Soutome Y, Ochi H, Umeda M, Higuchi T, Tanaka C. Correction of eddy currents for time-domain-interleaved blipped-phase-encoding echo-planar spectroscopic imaging. In: Proceedings of the 18th Annual Meeting of the International Society for Magnetic Resonance Imaging, Stockholm, Sweden, 2010. p 962.
104. Chu R, Madore B, Panych LP, Maier S. Parallel line scan diffusion imaging. In: Proceedings of the 16th Annual Meeting of ISMRM, Toronto, Canada, 2008, p 761.
105. Bito Y, Shirai T, Hirata S, Taniguci Y, Hirata K, Otake Y, Soutome Y, Ochi H, Ebisu T, Kawai Y, Umeda M, Higuchi T, Tanaka C. Parallel line-scan echo-planar spectroscopic imaging. In: Proceedings of the 17th Annual Meeting of ISMRM, Hawaii, USA 2009, p 2737.

CHAPTER 7 MAJOR ACHIEVEMENTS

7.1 PUBLICATIONS

7.1.1 PEER-REVIEWED PAPERS

Primary Author

1. Bito Y, Hirata S, Nabeshima T, Yamamoto E. Echo-planar diffusion spectroscopic imaging. Magn Reson Med 1995;33(1):69-73.
2. Bito Y, Ebisu T, Hirata S, Takegami T, Yamamoto Y, Tanaka C, Naruse S. Lactate discrimination incorporated into echo-planar spectroscopic imaging. Magn Reson Med 2001;45:568-574.
3. Bito Y, Hirata K, Ebisu T, Kawai Y, Otake Y, Hirata S, Shirai T, Soutome Y, Ochi H, Yamamoto E, Umeda M, Higuchi T, Tanaka C. Diffusion-weigted line-scan echo-planar spectroscopic imaging technique to reduce motion artifacts in metabolited diffusion imaging. Magn Reson Med Sci 2015;14:43-50.

Co-author

1. Taniguchi Y, Nakaya C, Bito Y, Yamamoto E. MRI high-speed simulator using transition matrix method and periodicity of magnetization. The IEICE Transactions (Japanese Edition) D 1994;J77-D2:566-572. [Japanese]
2. Hirata S, Bito Y, Yamamoto E. Expansion of the spectral bandwidth by spatial and chemical shift selective saturation in high-speed magnetic resonance spectroscopic imaging. Magn Reson Med 1996;35:611-616.
3. Takegami T, Ebisu T, Bito Y, Hirata S, Yamamoto Y, Tanaka C, Naruse S,

Mineura K. Mismatch between lactate and the apparent diffusion coefficient of water in progressive focal ischemia. NMR Biomed 2001;14:5-11.

4. Fujii S, Yamamoto E, Taniguchi Y, Bito Y. Development of a high-speed diffusion-weighted MRI simulator based on the Bloch-Torrey equation. Japanese Journal of Magnetic Resonance in Medicine 2013;33:1-12. [Japanese]
5. Tsukada K, Kusaka T, Saari MM, Takagi R, Sakai K, Kiwa T, Bito Y. Magnetic susceptibility and magnetic resonance measurements of the moisture content and hydration condition on a magnetic mixture material. J Appl Phys 2014;115:17E301
6. Otake Y, Soutome Y, Hirata K, Ochi H, Bito Y. Double-tuned RF coil design for ^{19}F and ^{1}H imaging. Magn Reson Med Sci, 2014;13:199-205.

7.1.2 OTHER PUBLICATIONS

Book

1. Bito Y, Ebisu T. Research application of diffusion imaging to small animal study: cerebral ischemia. In: Aoki S, Abe O, Masutani Y, Takahara T, editors. Diffusion MRI: Gakken Medical Syoujun-sya 2013; p. 144-145. [Japanese]

Review article

2. Bito Y, Okajima K, Koizumi H. Magnetic resonance imaging for biological function measurement. Japanese Journal of Analytical Chemistry “Bunseki” 1996;4:285-292. [Japanese]

7.2 PRESENTATIONS AT INTERNATIONAL CONFERENCES

Primary Author

1. Bito Y, Sekihara K. Reduction of truncation artifacts by using modified linear prediction. In: Proceedings of the 11th Annual Meeting of the Society for Magnetic Resonance, Berlin, Germany, 1992. p 422.
2. Bito Y, Hirata S, Yamamoto E. Four-dimensional echo-planar diffusion spectroscopic imaging. In: Proceedings of the 3rd Annual Meeting of the Society for Magnetic Resonance in Medicine, Nice, France, 1995. p 910.
3. Bito Y, Hirata S, Yamamoto E. Optimum gradient factor for apparent diffusion coefficient measurements. In: Proceedings of the 3rd Annual Meeting of the Society for Magnetic Resonance in Medicine, Nice, France, 1995 In: Proceedings the 3rd Annual Meeting of the Society for Magnetic Resonance in Medicine, Nice, France, 1995. p 913.
4. Bito Y, Hirata S, Tsukada K. Echo-planar diffusion spectroscopic imaging: reduction of motion artifacts using line-scan technique. In: Proceedings of the 6th Annual Meeting of the International Society for Magnetic Resonance Imaging, Sydney, Australia, 1998. p 1235.
5. Bito Y, Ebisu T, Hirata T, Takegami Y, Yamamoto Y, Tanaka C, Naruse S. Fast lactate-discriminating spectroscopic imaging using J-coupling in lactate and the broad spectral bandwidth of lipid. In: Naruse S, Watari H, editors. Ultrafast Magnetic Resonance Imaging. Amsterdam: Elsevier; 1999. p 259-262.
6. Bito Y, Tamura M. Feasibility study on ^{17}O-labeled contrast agent for MRI: phantom experiments. In: Proceedings of the 4th Annual Meeting of the Society for Molecular Imaging, Cologne, Germany, 2005. p 074.

7. Bito Y, Hirata S, Shirai T, Taniguchi Y, Ochi H. A spatio-spectral edge-preserving filter for magnetic resonance spectroscopic imaging. In: Proceedings of the 5th Annual Meeting of the Society for Molecular Imaging, Hawaii, USA, 2006. p 264.
8. Bito Y, Hirata S, Taniguchi Y, Shirai T, Ochi H. Spatio-spectral non-linear filtering of spectroscopic imaging: increasing signal-to-noise ratio while preserving spatial and spectral structure. In: Proceedings of the 15th Annual Meeting of the International Society for Magnetic Resonance Imaging, Berlin, Germany, 2007. p 1230.
9. Bito Y, Hirata K, Shirai T, Yamamoto Y, Soutome Y, Ebisu T, Umeda M, Kawai Y, Higuchi T, Tanaka C. Lactate-discriminating echo-planar spectroscopic imaging. In: Proceedings of the 16th Annual Meeting of the International Society for Magnetic Resonance Imaging, Toronto, Canada, 2008. p 596.
10. Bito Y, Hirata K, Ebisu T, Kawai Y, Otake Y, Hirata S, Shirai T, Soutome Y, Ochi H, Umeda M, Higuchi T, Tanaka C. Diffusion-weighted line-scan echo-planar spectroscopic imaging for improved accuracy in metabolite diffusion imaging. In: Proceedings of the 17th Annual Meeting of the International Society for Magnetic Resonance Imaging, Honolulu, USA, 2009. p 334.
11. Bito Y, Shirai T, Hirata S, Taniguchi Y, Hirata K, Otake Y, Soutome Y, Ochi H, Ebisu T, Kawai Y, Umeda M, Higuchi T, Tanaka C. Parallel line-scan echo-planar spectroscopic imaging. In: Proceedings of the 17th Annual Meeting of the International Society for Magnetic Resonance Imaging, Honolulu, USA, 2009. p 2737.
12. Bito Y, Hirata K, Ebisu T, Kawai Y, Otake Y, Hirata S, Shirai T, Soutome Y, Ochi

H, Umeda M, Higuchi T, Tanaka C. Motion artifact reduction using bipolar diffusion gradients in diffusion-weighted echo-planar spectroscopic imaging. In: Proceedings of the 18th Annual Meeting of the International Society for Magnetic Resonance Imaging, Stockholm, Sweden, 2010. p 24.

13. Bito Y, Hirata K, Ebisu T, Kawai Y, Otake Y, Hirata S, Shirai T, Soutome Y, Ochi H, Umeda M, Higuchi T, Tanaka C. Water suppression for diffusion-weighted line-scan echo-planar spectroscopic imaging. In: Proceedings of the 18th Annual Meeting of the International Society for Magnetic Resonance Imaging, Stockholm, Sweden, 2010. p 959.
14. Bito Y, Hirata K, Hirata S, Shirai T, Ebisu T, Kawai Y, Otake Y, Soutome Y, Ochi H, Umeda M, Higuchi T, Tanaka C. Correction of eddy currents for time-domain-interleaved blipped-phase-encoding echo-planar spectroscopic imaging. In: Proceedings of the 18th Annual Meeting of the International Society for Magnetic Resonance Imaging, Stockholm, Sweden, 2010. p 962.
15. Bito Y, Hirata K, Hirata S, Shirai T, Ebisu T, Kawai Y, Otake Y, Soutome Y, Ochi H, Umeda M, Higuchi T, Tanaka C. Diffusion-weighted spectroscopic imaging: techniques for reducing motion artifacts. In: Proceedings of the Ultra-high Field Systems & Applications: 7T & Beyond: Progress, Pitfalls & Potential, International Society for Magnetic Resonance Imaging Scientific Workshop, Lake Louise, Canada, 2011. Poster #5.
16. Bito Y, Kawai Y, Hirata K, Ebisu T, Shirai T, Hirata S, Soutome Y, Ochi H, Umeda M, Higuchi T, Tanaka C. Diffusion-weighted spectroscopic imaging of rat brains after middle cerebral artery occlusion. In: Proceedings of the 19th Annual Meeting of the International Society for Magnetic Resonance Imaging, Montreal,

Canada, 2011. p 143.

17. Bito Y, Kawai Y, Hirata K, Ebisu T, Shirai T, Hirata S, Soutome Y, Ochi H, Umeda M, Higuchi T, Tanaka C. Diffusion tensor spectroscopic imaging of rat brains. In: Proceedings of the 19th Annual Meeting of the International Society for Magnetic Resonance Imaging, Montreal, Canada, 2011. p 408.
18. Bito Y, Kawai Y, Hirata K, Ebisu T, Shirai T, Hirata S, Soutome Y, Ochi H, Umeda M, Higuchi T, Tanaka C. Diffusion-weighted spectroscopic imaging of multiple metabolites in rat brains after middle cerebral artery occlusion. In: Proceedings of the 20th Annual Meeting of the International Society for Magnetic Resonance Imaging, Melbourne, Australia, 2012. p 3596.
19. Bito Y, Kawai Y, Hirata K, Ebisu T, Shirai T, Hirata S, Soutome Y, Ochi H, Umeda M, Higuchi T, Tanaka C. Diffusion tensor spectroscopic imaging of multiple metabolites in rat brains. In: Proceedings of the 21st Annual Meeting of the International Society for Magnetic Resonance Imaging, Salt Lake City, USA, 2013. p 3955.
20. Bito Y, Kawai Y, Hirata K, Ebisu T, Shirai T, Hirata S, Soutome Y, Ochi H, Umeda M, Higuchi T, Tanaka C. Diffusion tensor spectroscopic imaging of multiple metabolites in rat brains. In: Proceedings of the Diffusion as a Probe of Neural Tissue Microstructure, International Society for Magnetic Resonance Imaging Scientific Workshop, Podstrana, Croatia, 2013. Poster #60.